Pro gradu

DNA damage sensitization of breast cancer cells with PARP10/ARTD10 inhibitor

Mikko Hukkanen

University of Oulu

Faculty of Biochemistry and Molecular Medicine

2019

This thesis was completed at the Faculty of Biochemistry and Molecular Medicine, University of Oulu.

Oulu, Finland

Supervisors:

Professor Lari Lehtiö, Dr. Jarkko Koivunen and MSc Sudarshan Murthy

Acknowledgements

The work of this thesis was made in Faculty of Biochemistry and Molecular Medicine (FBMM) of University of Oulu.

Firstly, I would like to thank Professor Lari Lehtiö for the opportunity working in his group, and the advice I received for my thesis. My gratitude is expressed also to my other supervisors, Jarkko Koivunen, for all the guidance I received in the cell culture, and Sudarshan Murthy, for the guidance to express and purify protein, and to conclude IC_{50} analysis.

I would also thank all the personnel in LL group for all the advice I received in laboratory. I would especially thank Sven Sowa who made the Mantis run for IC_{50} analysis possible.

Abbreviations

5-FU – 5-fluorouracil
aa – Aminoacid
ADP – Adenosine diphosphate
ADPr – ADP-ribosylation
AEC – Anion-exchange chromatography
AIF – Apoptosis inducing factor
AIM – Auto-induction medium
Arg – Arginine
ART – ADP-ribosyltransferase
ARTD – Diphtheria toxin –like ADP-ribosyltransferase
Asp – Aspartate
BRCA – Breast cancer gene
BRCT – BRCA1 C terminus
CPT – Camptothecin
CRC – Colorectal cancer
CRM1 – Chromosome region maintenance 1
Cys – Cysteine
DDR – DNA damage response
dH_2O – Distilled water
DMEM – Dulbecco's modified eagle's medium
DMSO – Dimethyl sulfoxide
DNA – Deoxyribonucleic acid
dNTP – Deoxynucleoside triphosphate
DSB – Double-strand break
ECL – Enhanced chemiluminescence
EDTA – Ethylenediaminetetraacetic acid
EGTA – Egtazic acid
EtOH – Ethanol
FBS – Fetal bovine serum
FdUMP – 5-fluoro-2′-deoxyuridine-5′-monophosphate

Glu – Glutamate

Gly – Glycine

HeLa – Henrietta Lacks

HEPES – 4-(2-hydroxyethyl)-1-piperazineethanesulfonic acid

HP – High performance

HRP – Horseradish peroxidase

HRR – Homologous replication repair

HU – Hydroxyurea

IC_{50} – Half maximal inhibitory concentration

IMAC – Immobilized metal ion affinity chromatography

IR – Ionizing radiation

kb – Kilobase

kDa – Kilodalton

KOH – Potassium hydroxide

Lys – Lysine

MAR – Mono-ADP-ribose

mARTD – Mono ARTD

MARylation – Mono-ADP-ribosylation

MCF7 – Michigan cancer foundation 7

MDA-MB-231 – M. D. Anderson metastasis breast cancer 231

MMR – Mismatch repair

MYC – Myelocytomatosis viral oncogene homolog

NaCl – Sodium chloride

NAD – Nicotinamide adenine dinucleotide

NEMO – Nuclear factor-kappa B essential modulator

NER – Nucleotide excision repair

NES – Nuclear export sequence

NF-kB – Nuclear factor-kappa B

nm – Nanometer

P/S – Penicillin/streptomycin

PAR – Poly-ADP ribose

PARP – Poly-ADP-ribose polymerase

PARPi – PARP inhibitor

pARTD – poly ARTD

PARylation – Poly-ADP-ribosylation

PBS – Phosphate buffer saline

PCNA – Proliferating cell nuclear antigen

pH – Potential of hydrogen

pI – Isoelectric point

PIP – PCNA-interacting peptide

Poly-his – Poly-histidine

PTM – Post-translational modification

pUb – Poly-ubiquitin

PVDF – Polyvinylidene fluoride

RBP – RNA binding pocket

RNA – Ribonucleic acid

RPE1 – Retinal pigmented epithelial cell 1

RRM – RNA recognition motif

SDS – Sodium dodecyl sulphate

SDS-PAGE – Sodium dodecyl sulphate polyacrylamide gel electrophoresis

SEC – Size-exclusion chromatography

SEM – Standard error of the mean

Ser – Serine

SRPK2 – Serine-rich protein-specific kinase 2

SSB – Single-strand break

SSBR/BER – Single-strand break repair/base excision repair

TBS – Tris-buffered saline

TCEP – Tris(2-carboxyethyl)phosphine

TEV – Tobacco etch virus

TG – Tris-glycine

TLS – Translesion synthesis

TPM – Transcripts per million

UIM – Ubiquitin-interaction motif

UV – Ultraviolet

Table of Contents

I LITERATURE SECTION

1. Introduction

1.1 ADP-ribosylation

Post-translational modifications (PTMs) play a crucial role in various mechanisms of cellular proliferation. Some of the PTMs can be divided to poly-ADP-ribosylation (PARylation) and mono-ADP-ribosylation (MARylation). The proteins that perform such PTMs are called poly-ADP-ribose polymerases (PARPs), also known as diphtheria toxin –like ADP-ribosyl transferases (ARTDs). As name indicates, MARylating PARP/ARTD-family proteins add only an ADP-ribose monomer, whereas PARylating PARP/ARTD-family proteins add a chain of ADP-ribose polymer to target proteins. PARylation and MARylation are important during several biological processes, such as gene transcription, stress response, heat shock for instance, response to unfolded protein, and deoxyribonucleic acid (DNA) damage response (DDR). (Flohr *et al.*, 2003; Siegel & McCullough, 2011; Vyas *et al.*, 2013; Liu & Yu, 2015)

The family of PARPs can be divided to 17 differently functioning proteins. This group can be divided to tankyrases, zinc-finger-, DNA-dependent- and unclassified PARPs. The PARylation/MARylation process itself requires ADP-ribose to function, as its name implicates, and it is acquired from nicotinamide adenine dinucleotide (NAD^+) by PARP/ARTD–family proteins. Furthermore, the ADP-ribosylation is required in DNA repair mechanisms. (Flohr *et al.*, 2003; Liu & Yu, 2015)

Not only are PARPs required for DNA repair mechanisms, but they can also commence non-caspase coordinated apoptosis. One example of such an event is an insurmountable cell stress, namely elevated oxygen radical levels continuously damaging DNA. In these types of DNA damaging events PAR is excessively formed, namely via PARP1 activity, leading to apoptosis inducing factor (AIF) release from mitochondria. Furthermore, the released AIF translocates into nucleus and induces apoptosis via chromatin condensation and DNA cleavage into 50 kilobase (kb) fragments. (Siegel & McCullough, 2011)

DNA damage is linked to cancer, and the ARTDs play a role in breast cancer, which is one of the most severe cancer in women. In some cases, this disease arises from two gene mutations in *BRCA1* and *BRCA2*. The inhibition of ARTDs with PARP inhibitors (PARPi), especially ARTD1, are noted to lead especially specific cell killing (Tutt *et al.*, 2010). Not only the PARPi has the potential to sensitize the cells to the DNA damage, but also the inhibitors can protect the cells from necrosis. One such PARPi preserving the cells is 3-aminobenzamide, which has been proven to decrease the follicular cell necrosis levels (Makogon *et al.*, 2010).

ARTDs has also a dual nature, both preserving and damaging cells, depending on the energy availability. If only a little of energy source (NAD^+ and ATP) is present, the ARTD activity lead to necrosis. In the other hand, if energy is available, DNA repairing enzymes are activated via ARTD, and thus the cells proliferate. (Putt & Hergenrother, 2004)

2. Review of the literature

2.1 Mono-ADP-ribosylation

A post-translational modification (PTM) is an event, which covers a series of covalent amino-acid side chain modifications. To date, 300 PTMs has been approximated to occur, and one of such events is called ADP-ribosylation. (Kumar & Prabhakar, 2008)

ADP-ribosyltransferases (ARTs) ADP ribosylate their target proteins. This PTM occurs during various regulation processes, including stress response, apoptosis, DNA damage repair and cell division. Also, it divides into mono-ADP-ribosylation (MARylation) and poly-ADP-ribosylaion (PARylation). (Bütepage *et al.*, 2015; Munnur & Ahel, 2017)

In a chemical level, ARTs use NAD^+ as a substrate for branching ADP ribose, with nicotinamide releasing as derivative. If there are no proteins to be ADP-ribosylated, free amino acids are capable to act as substrates. If no free amino acids are present, the NAD^+ is slowly hydrolyzed to ADP ribose and nicotinamide. On figure 1, the ADP-ribosylation is represented. (Han *et al.*, 1996; Berti *et al.*, 1997; Bütepage *et al.*, 2015)

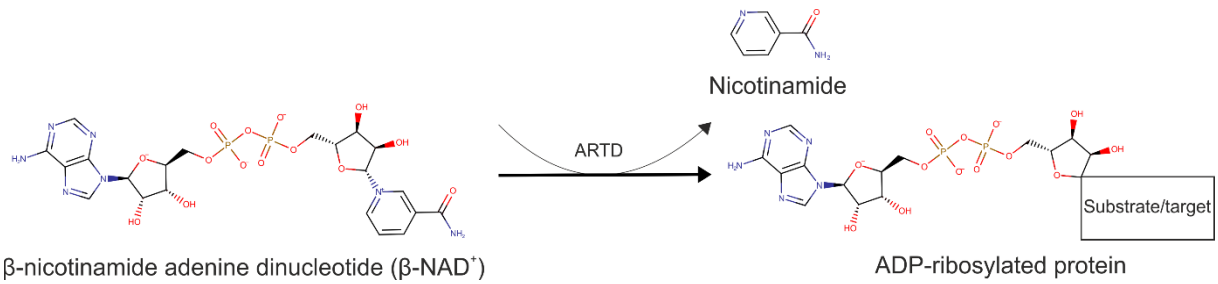

Figure 1: An overview of ADP-ribosylation. On this schematic, β-NAD^+ is utilized into ADP-ribose via ARTD activity.

ARTs target their ADP-ribosylation on several amino-acids. Most common targets are aspartate (Asp), glutamate (Glu), and serine (Ser). Other residues to be ADP-ribosylated are arginine (Arg), cysteine (Cys) and lysine (Lys). One of the target proteins undergoing the ADP-ribosylation are histones. Upon DNA damage, PARP-family proteins target histones, namely

ARTD1 and ARTD2, from which ARTD1 targets primarily histone H1 (linker histone), and ARTD2 targets core histones, such as H2B. The ADP-ribosylation of histones cause the chromatin structure relaxation, facilitating the single-strand break repair/base excision repair (SSBR/BER) factors to the DNA damage site. However, it is unclear which specific site of the histones become PARylated. (Herceg & Murr, 2011; Feijs *et al.*, 2013; Leidecker *et al.*, 2016; Rakhimova *et al.*, 2017; Bartlett *et al.*, 2018)

On table I, a list of PARP-family proteins with ARTD-name and suggested activity type is represented. (Vyas *et al.*, 2014; Yang *et al.*, 2017)

Table I: A list of ARTDs.

PARP	ARTD	Activity
PARP1/PARP	ARTD1	PAR
PARP2	ARTD2	PAR
PARP3	ARTD3	MAR
PARP4/vPARP	ARTD4	MAR
TNKS1	ARTD5	PAR
TNKS2	ARTD6	PAR
PARP6	ARTD17	MAR
PARP7/tiPARP	ARTD14	MAR
PARP8	ARTD16	MAR
PARP9/BAL1	ARTD9	MAR
PARP10	ARTD10	MAR
PARP11	ARTD11	MAR
PARP12	ARTD12	MAR
PARP13/ZC3HAV1	ARTD13	Inactive
PARP14/BAL2	ARTD8	MAR
PARP15/BAL3	ARTD7	MAR
PARP16	ARTD15	MAR

2.2 PARP10/ARTD10

Poly-ADP-Ribose Polymerase 10 (PARP10), or Diphtheria Toxin –like ADP-ribosyltransferase (ARTD10), is expressed in all tissues, and it interacts with at least 8000 proteins. In humans, ARTD10 interferes with activities of various cellular proteins via MARylation. Few examples of the target proteins of ARTD10 are growth factors, receptors and different kinases. The PTM of these proteins makes regular cell proliferation possible. However, it has been noticed that inhibition of overexpressed ARTD10 aid cells to proliferate. (Feijs *et al.*, 2013; Nicolae *et al.*, 2014; Bütepage *et al.*, 2015; Ekblad *et al.*, 2015; Venkannagari *et al.*, 2016)

Generally, the modification by ARTD10 leads to an inhibition of protein activity in a cellular signaling pathways. One of such pathways is a nuclear factor-kappa B essential modulator (NEMO) pathway, which require K63-pUb to be activated. ARTD10 can prevent the activation of this pathway via binding to K63-pUb with its two ubiquitin-interaction motifs (UIMs). (Verheugd *et al.*, 2013; Bütepage *et al.*, 2015)

ARTD10 is suggested to act as an oncogene, promoting the tumor growth. Also, loss of this enzyme has been noted to reduce cancer cell proliferation, thus the inhibition of ARTD10 is a promising method of anti-cancer therapy. (Schleicher *et al.*, 2018)

2.2.1 Structure of ARTD10

ARTD10 consists of various regions, which all have important roles in cellular processes. It has a region containing motif designed to recognize RNA, an RNA recognition motif (RRM, amino acids (aa) 11-85). This motif has various regulation targets amongst different RNA sequences, and it occurs via group of specified RNA binding proteins (RBPs). Other regions ARTD10 consists of are glycine-rich region (Gly, aa 281-399) , nuclear uptake mediating conserved nuclear targeting region (aa 435-528), glutamine-rich region (Glu, aa 588-697) including Nuclear Export Sequence (NES, aa 598-607), which is suggested to have a role in nuclear localization, and two Ubiquitin-Interacting-Motifs (UIMs, aa 650-667 and 673-690), which attach to ubiquitinated molecules such as proliferating cell nuclear antigen (PCNA) upon

replication fork stalls. The distinguishable catalytic domain (aa 818-1013) and PCNA-interacting peptide (PIP-box, aa 834-841) box of ARTD10 are located at C-terminus. This domain is region in which MARylation of target proteins occur. On figure 2, an overview of ARTD10 structure is represented. (Yu *et al.*, 2005; Kleine *et al.*, 2008; Yu *et al.*, 2011; Herzog *et al.*, 2013; Verheugd *et al.*, 2013; Nicolae *et al.*, 2014; Bock *et al.*, 2015; Schleicher *et al.*, 2018).

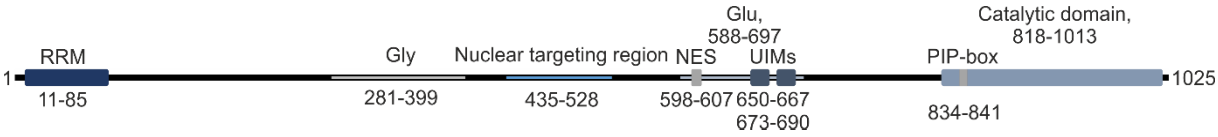

Figure 2: An overview of ARTD10. On this graphical representation, different regions of full-length human ARTD10, a 1025 amino acids long protein, can be seen.

2.2.2 ARTD10 response to DNA damage

DNA is exposed constantly to exo- and endogenous damages. To maintain regular activity of cells, a variety of DNA repair mechanisms must act correctly. If repair mechanisms are unable to treat DNA properly, several different genomic anomalies will occur, namely chromosomal translocations, gain or loss of entire chromosomes, and point mutations. Furthermore, if multiple repair mechanisms of DNA become altered, a tumorigenesis will occur due to unsuccessful DNA damage repairing. (Mouw *et al.*, 2017)

One of the ARTD10 properties is to translocate between compartments of cytoplasm and nucleus, but it is not completely clear how its translocation occurs. Kleine H. and colleagues (2012) has discovered that the nuclear ARTD10 potentially interacts with myelocytomatosis viral oncogene homolog (MYC) and the shuttling is mediated with NES region binding chromosome region maintenance 1 (CRM1) -dependent nuclear export sequence and a central nuclear localization promoting sequence of ARTD10. However, the nuclear localization region of ARTD10 does not provide full nuclear translocation. ARTD10 is distributed equally between nuclear compartments and cytoplasm, and it is suggested the co-localization between cytoplasm

and nucleus occurs with p62/SQSTM1, a pUb receptor. (Kleine *et al.*, 2012; Herzog *et al.*, 2013)

A phenomenon called DNA damage response (DDR) alters the chromatin structure. This affects epigenetic marks as well as essential chromatin factors, with crucial connections for functions of epigenome. The chromatin goes through a tense spatio-temporal regulation. It has been noticed that the chromatin relaxation occurs at DNA break sites, followed by temporary compaction. (Nicolae *et al.*, 2014; Dabin *et al.*, 2016)

One of the consequences of DNA damages are DNA lesions. If DNA lesions remain unrepaired, the DNA will eventually break. The known mechanisms responding to DNA damage include nucleotide excision repair (NER), translesion synthesis (TLS), base excision repair, mismatch repair. ARTD10 have been identified to act as a component of TLS mechanism. ARTD10 is actively taking part in these repair mechanisms during S-phase, and it have been noted the cells lacking ARTD10 are uncapable to restart DNA replication after DNA damage specified to S-phase. (Nicolae *et al.*, 2014; Shahrour *et al.*, 2016)

A ring-like PCNA is a polymerase δ cofactor, and it surrounds the DNA strand during synthesis recruiting DNA repair- and replicator proteins (Peterson & Kovyrshina, 2019). Upon DNA damaging events, one of the recruited proteins is ARTD10, which is recruited via its exclusive PIP-box. It is shown before that ARTD10 can bind to PCNA with either PIP-box or UIMs, which binds to ubiquitinated PCNA. Also, the binding with UIMs and PIP-box occurs respectively. Nicolae and colleagues suggest the genomic stability is promoted via recruitment of ARTD10 to replication fork stalls, speculating this activity might have a role in DNA repair. The recruitment is vital, since DNA anomalies, such as repetitive elements, lesions, secondary structures and further non-canonical structures, will eventually seize the progression of DNA polymerases. The replication fork arrest leads to PCNA mono-ubiquitination at Lys164. The ubiquitination will eventually promote recruitment of UIM –and PIP-box possessing TLS polymerases, culminating to stalled fork restart (Nicolae *et al.*, 2014; Schleicher *et al.*, 2018).

The overexpression of ARTD10 have been identified in a broad spectrum of tumors, and thus it might have a role as an oncogene in transformation promotion. However, when overexpressed, ARTD10 is known to induce apoptosis in HeLa-cells. Schleicher and colleagues (2018) noted the overexpression of ARTD10 led to enhanced growth of RPE-1 -cells, and the overexpression of catalytic domain did not have effect on cellular proliferation. In the contrast,

the downregulation of ARTD10 is known to result into various neurodegenerative disorders such as Cockayne syndrome, PCNA mutation, xeroderma pigmentosum, and ataxia telangiectasia. Shahrour and colleagues (2016) discovered a neurodegenerative disease via ARTD10 deficiency, which led to increased apoptosis levels due flawed DNA repair mechanism (Herzog *et al.*, 2013; Shahrour *et al.*, 2016; Schleicher *et al.*, 2018).

2.3 ARTDs in DNA damage response

A common feature of ARTD-family proteins is the ADP-ribosylation, which is suggested to have a role during dsDNA damage repair, such as single-strand breaks (SSBs). As a part of DNA repair mechanism, ARTDs are targeting histones H3 and H4 upon DNA stress. As an example, histone H3 is removed from DNA damage site due PARylation, granting DNA repair space. Once histones H3 and H4 are PARylated, the acetylation levels of the tails are increased. Thus, it is suggested that PARylation allows constitutive transcription maintenance due preventing histone deacetylation. However, if amount of poly(ADP-ribose) is either extensive or restricted, histones become hypoacetylated. (Flohr *et al.*, 2003; Verdone *et al.*, 2015; Chen *et al.*, 2018)

2.3.1 Activity on DNA damage sites

In a summary, ARTD-dependent pathways of DNA damage repair activity can be divided in three different categories, which are DNA damage detection, PAR-dependent repair factor recruitment, and PAR-dependent biochemical activity regulation. Upon SSBs, ARTDs binds to specific ends via zinc finger domains. These domains bind mutually, instead of competing for the same binding site. Furthermore, ARTD binds to a damaged DNA site as a monomer, and the positioning of heavily modified ARTD region, consisting of linker residues that subsequent BRCA1 C terminus (BRCT) fold, is dependent on domain organization. Finally, the allosteric activation of ARTD requires reorganization of the helical HD domain. The HD blocks the catalytic domain from NAD+ binding, and the deletion of HD renders ARTD1, ARTD2, and ARTD3 active. These proteins are activated upon different DNA damage, ARTD2 and ARTD3

being activated most in the cases upon 5´ terminal DNA phosphorylation and SSBs whereas ARTD1 is activated mostly upon double-strand breaks (DSBs). Also, ARTD1 assembles on DNA via PAR-mediated automodification, which lead eventually ARTD1 to unbind DNA whilst decreasing catalytic output. However, the ratio between ARTD1 mediated repair factor recruiting and ARTD1 unbinding automodifications is not clear. The complex of DNA repairing factors relies to a sophisticated network consisting of protein-protein and protein-DNA contacts. One such an interaction is histone PARylation factor 1 (HPF1), which is identified as an ARTD1 binding counterpart, regulating the catalytic output. (Trucco *et al.*, 1998; D'Amours *et al.*, 1999; Sukhanova *et al.*, 2005; Langelier *et al.*, 2012; Dawicki-McKenna *et al.*, 2015; Eustermann *et al.*, 2015; Gagné *et al.*, 2015; Gibbs-Seymour *et al.*, 2016; Liu *et al.*, 2017)

2.4 PARP inhibitors in DNA damage

PARPi possesses promising clinic anti-cancer activity. The effect relies on DNA repair mechanism inhibition and thus enhance the effects of anti-cancer therapy, namely topoisomerase I poisons, ionizing radiation (IR) and DNA methylating agents. These damages are enhanced, since the ARTD inhibition reduces poly(ADP-ribose) (PAR) chain synthesis and thus, seizes additional repair factor recruitment. (Gavande N. S. *et al.*, 2016)

A few examples of hypersensitization are the cells possessing imperfect DNA mismatch repair (MMR), homologous replication repair (HRR) mechanism, or lacking ARTDs. This makes treatment of tumors emerged from breast cancer gene (BRCA) mutation carrying cells effective, since the PARP1- and PARP2 inhibitors kills HRR imperfect cells via synthetic lethality between PARPi and defects in HRR mechanism. (Curtin & Szabo, 2013; Morgan *et al.*, 2015; Gavande *et al.*, 2016; Bian *et al.*, 2019).

2.4.1 PARP inhibitors

Once the ARTDs were discovered, PARPi have been developed to bind specifically in active sites of ARTDs, such as NAD^+ binding site. The modern PARPi are NAD^+ competitors,

occupying catalytic pockets of ARTDs. Examples of such PARPi are Olaparib (AZD-2281), rucaparib, veliparib, niraparib and talazoparib, which are ARTD1, ARTD2- and ARTD3 inhibitors. These inhibitors inhibit the enzymatic activity, including automodification, and trap the enzyme to DNA strand. The overall effect on cells are arrest of cell cycle, especially at G2/M checkpoint, and the cells are known to be radiosensitive during this phase. Also, these chemicals enhance the potency of DNA-damaging agents such as cisplatin (Curtin & Szabo, 2013; Gavande *et al.*, 2016; Dockery *et al.*, 2017; Prasad *et al.*, 2017; Bian *et al.*, 2019; Camero *et al.*, 2019).

2.4.2 Mono-ARTD inhibitors

The inhibitors targeting mono-ARTDs (mARTDs) are gathering more interest for their advantageous properties, as mARTDs are now known to take part in several cellular processes. As a common feature with other PARPi, mARTD inhibitors so far possess a nicotinamide-mimicking characteristic, competing with substrate NAD+ and preventing the enzymatic activity. However, challenges in developing the mARTD inhibitors lies on selectivity as well as potency exists, and more efforts to discover specific compounds are needed. Catalytic domain is highly conserved in ARTD family proteins and therefore compounds often inhibit multiple enzymes. At a moment, research groups are at an early-hit development phase, such as research groups of Schuller (2017), Holechek (2018), and Morgan (2019), primary seeking appropriate ARTD8 inhibitor, and due this fresh frontier of PARPi studies, there is not yet data from clinical trials. At a moment, one example of specific mARTD inhibitor is OUL35, which inhibits specifically ARTD10. (Ekblad *et al.*, 2015; Venkannagari *et al.*, 2016; Schuller *et al.*, 2017; Holechek *et al.*, 2018; Morgan *et al.*, 2019)

2.4.2.2 OUL35

OUL35 (4-(4-carbamoylphenoxy)benzamide, (NSC39047)), is a recently discovered inhibitor of ARTD10, by Lehtiö group. By docking studies, it was found that OUL35 binds same way as 3AB, a small general ARTD inhibitor, by binding in the NAD^+ binding pocket. They also noted

that the OUL35 -treated ARTD10-overexpressing HeLa cells were rescued from ARTD10-induced apoptosis. (Venkannagari *et al.*, 2016)

On figure 3, structures of Olaparib and OUL35 is shown. The NAD^+ mimicking regions are highlighted with transparent gray circles. As recognizable differences, Olaparib is extending towards the adenosine-binding pocket along NAD^+ binding branch, whereas the benzamide motif of OUL35 is extending towards the acceptor from the NAD^+ binding pocket. (Dawicki-McKenna *et al.*, 2015; Venkannagari *et al.*, 2016)

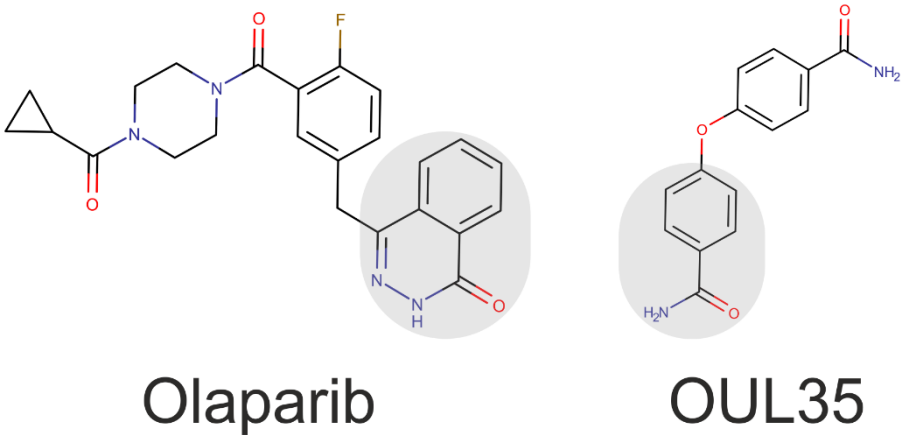

Figure 3: A comparison between Olaparib and OUL35.

2.5 DNA damaging chemotherapeutics

DNA can be damaged by many means, both exo- and endogenous. Exogenous damage is broadly used in radiation therapy and chemotherapy, which lead to various DSBs, SSBs, base damages and termini modifications. The key aspect of chemotherapy is to use synergetic compounds together to provide most effective cancer-eradication, and to extend the effectiveness of treatment even more, simultaneous repair mechanism inhibition can be used. The compounds modifying specifically DNA bases chemically dates to 1960s and 1970s. During those days, one of the most efficacious anti-cancer drugs, platinum agents bearing alkylating-like properties, were found, and amongst the found compounds, cisplatin is one of the most successful one. The chemotherapy treatment is utilized broadly amongst various cancer types alongside surgical procedures, attempting to effectively eradicate cancer. The

previously mentioned cisplatin is effective to a certain extent, but it generates severe side-effects to the patients, namely nephro- neuro- and hepatotoxicity. Moreover, the cancer cells either possesses or develops resistance to this compound. Thus, it is important to develop different drug combinations, and cisplatin has been developed furthermore ever since into thousands of different analogs. The combination chemotherapy has requirements itself as well, namely enhancing the cancer cell kill effectiveness, non-overlying toxicity and cancer resistance avoidance, since if the tumor develops a resistance to a drug, reoccurrence of disease will be a matter of time. Also, the importance of ARTDs should not be ignored. It is known that in regular cellular conditions, when enough energy is stored, PARPi prevent the ARTD-mediated DNA repairing protein recruitment. Nicolae and colleagues (2014) suggest that the cells may utilize ARTD10 to decrease the effects of DNA-damaging chemotherapeutics, and thus preventing the full effect of anticancer drugs. Nevertheless, the chemotoxicity resistance based on ARTD10 activity can be prevented with target-specific inhibitors, which are constantly being studied and developed. (Putt & Hergenrother, 2004; Bruijnincx & Sadler, 2008; Cheung-Ong *et al.*, 2013; Nicolae *et al.*, 2014; Gavande *et al.*, 2016; Hu *et al.*, 2016)

II EXPERIMENTAL PART

3. Aim of the project

The key aspects of this projects were

1) to express and purify recombinant full length ARTD10,

2) to conduct IC_{50} experiments on ARTD10 to compare values between full length protein and catalytic fragment used previously,

3) to determine the effects of DNA damaging agents as well as OUL35 on ARTD10 levels and localization in cells, and

4) to determine whether the OUL35 increases the effects of DNA damaging agents on breast cancer cells and whether there is correlation with ARTD10 expression levels

4. Materials and methods

4.1 Protein expression

The ARTD10 expressing plasmid was transformed previously to bacteria, which was inoculated from glycerol stocks of frozen *E. coli* Rosetta 2 (DE3) –cells. The strain possessed the ARTD10 encoding sequence in pNIC-Bsa4 –plasmid with poly-his tag and tobacco etch virus (TEV) protease recognition sequence. Preliminary culture used consisted of 5 ml of LB broth (Lysogeny Broth; 25% LB broth Miller, dH_2O). The antibiotics were kanamycin (50 µg/ml) and chloramphenicol (37 µg/ml), and the cells were incubated overnight in +37°C shaking incubator.

The overnight culture was inoculated into secondary culture of autoclaved auto-induction medium (AIM; 5% Formedium Auto Induction Terrific Broth), and the cells were incubated in a 5 l Erlenmeyer flask, with final volume of 750 ml, at shaking +37 °C incubator. With two-hour intervals, OD600 value was checked with spectrophotometer. Once the OD600 reached 1.0, incubator temperature was lowered to +18 °C, and let the cells grow overnight (16h).

After 16 h incubation, the cells were spun down with 4200 rpm (Beckman J6-MI Centrifuge, JS-42 rotor, Beckman tubes) for 30 minutes (+4 °C). After centrifuging, pellets were weighed, and lysis buffer was added (1.5 ml/g pellet) (50 mM HEPES, 500 mM NaCl, 10% glycerol, 10 mM imidazole, 0.5 mM TCEP, pH 7.8). The cells were lysed using cell disruptor with pressure of 20 kpsi (Constant Systems Ltd). Two passes were required to successfully lyse the cells.

4.2 Protein purification

The used methods for ARTD10 were immobilized metal ion affinity chromatography (IMAC), anion-exchange chromatography (AEC) and finally, size-exclusion chromatography (SEC). Before initiating the IMAC purification, the lysate was filtered using 0.45 µM filter (Sartorius). Centricon (30 kDa) was used to obtain appropriate protein solution volume after IMAC. Furthermore, sodium dodecyl sulphate polyacrylamide gel electrophoresis (SDS-PAGE) was

used to check the purity level of eluate obtained from chromatography, and as a standard, Precision Plus Protein All Blue Standards (BioRad, 250-10 kDa) was used.

IMAC is based most commonly on poly-histidine (poly-his) -tail protein affinity to a metal ion saturated column, in the case of this work, nickel. The cells are firstly lysed with, for example, cell disruptor and the obtained lysate is filtered. Once the lysate is filtered from cell debris, it is passed through an IMAC column. The following steps consists of column washes using washing buffers with different concentrations of imidazole. Elution Buffer has the highest concentration of imidazole, rinsing away almost everything off the column. The imidazole competes with histidine in binding to nickel, resulting poly-his -and other nickel-binding proteins rinse away.

IMAC column used for purification was pre-packed high-performance (HP) IMAC column (GE healthcare). The used washing buffers were Wash 1 (30 mM 4-(2-hydroxyethyl)-1-piperazineethanesulfonic acid (HEPES), 350 mM NaCl, 10 mM Imidazole, 10% glycerol, 0,5 mM Tris(2-carboxyethyl)phosphine (TCEP), pH 7.5), Wash 2 (30 mM HEPES, 350 mM NaCl, 25 mM Imidazole, 10% glycerol, 0.5 mM TCEP, pH 7.5) and Elution Buffer (30 mM HEPES, 350 mM NaCl, 350 mM Imidazole, 10% glycerol, 0.5 mM TCEP, pH 7.5).

If protein of interest interacts with nucleic acids, one can remove the contaminating RNA or DNA with heparin chromatography. This was made with buffer A (25 mM Tris, 50 mM NaCl, pH 7.6), and the column of this purification step was HiTrap Heparin HP column (GE healthcare).

The matrix of AEC consists of beads of cross-linked agarose having strong anion-exchange properties. The charge is dependent on potential of hydrogen (pH) value (effects on isoelectric point (pI) as well), and the oppositely charged molecules attracts each other resulting protein binding on column. The protein is washed away as fractions with buffers, Buffer A and Buffer B typically, due charge changes of the column by change of sodium chloride (NaCl) gradient. The column used for AEC was Q-sepharose and the buffers used for elution were Buffer A (25 mM Tris, 50 mM NaCl, pH 7.6) and Buffer B (25 mM Tris, 1 M NaCl, pH 7.6).

The molecules passed through SEC column do not bind to the medium, but the proteins are separated according to the size. The larger the protein, the faster it passes through the column. The proteins are eluted from the column with Gel Filtration Buffer (30 mM HEPES, 350 mM NaCl, 10% glycerol, 0.5 mM TCEP, pH 7.5) and the wanted protein is collected in different

fractions. In case of full-length PARP10, S200 column was used (Superdex, resolve (M_r) from 10 000 to 600 000) with matrix consisting of a cross-linked spherical composite of dextran and agarose.

4.3 Activity assay and inhibitory potency measurements

A fluorescence-based activity assay was performed to seek the appropriate concentration of inhibitor, OUL35, to complete ARTD10 inhibition, using serine-rich protein-specific kinase 2 (SRPK2) as a substrate. The assay was made in 96-well plates (Venkannagari *et al.*, 2013). On table II, the layout of the contents is represented.

Table II: Layout of half maximal inhibitory concentration (IC_{50}). Well column 1 has 50 µl 50 mM Tris buffer as a blank, column 2 acts as a negative control and column 12 is a positive control. Wells 3-11 separates into two parts, having upper 4 wells as a control's wells without PARP10.

<table>
<tr><th></th><th>1</th><th>2</th><th>3</th><th>4</th><th>5</th><th>6</th><th>7</th><th>8</th><th>9</th><th>10</th><th>11</th><th>12</th></tr>
<tr><td>A</td><td rowspan="8">50 mM Tris</td><td rowspan="2">25 µl
1 µM</td><td colspan="9" rowspan="4">25 µl
1 µM NAD+</td><td rowspan="2">25 µl
1 µM NAD+</td></tr>
<tr><td>B</td></tr>
<tr><td>C</td><td colspan="9" rowspan="2">10 µl
50 mM Tris</td></tr>
<tr><td>D</td><td rowspan="2">5 µl
1%</td><td rowspan="2">10 µl
2 µM SRPK2</td></tr>
<tr><td>E</td><td colspan="9" rowspan="4">1 – 100 µM OUL35</td></tr>
<tr><td>F</td><td rowspan="2">10 µl
50 mM</td><td rowspan="2">10 µl
150 nM PARP10</td></tr>
<tr><td>G</td><td colspan="9" rowspan="2">25 µl
1 µM NAD+
10 µl 150 nM ARTD10</td></tr>
<tr><td>H</td><td rowspan="2">10 µl
2 µM</td><td rowspan="2">5 µl 1% DMSO</td></tr>
<tr><td></td><td colspan="9">10 µl
2 µM SRPK2
1 – 100 µM OUL35</td></tr>
</table>

NAD^+ is consumed as in the enzymatic reaction. The reaction occurs on 96-well plate in shaking incubator, which keeps the temperature constant overnight. The following day the reaction is halted by denaturing the proteins with 2 M potassium hydroxide (KOH), which also makes the conditions basic. Straightly after denaturing the protein, 20% acetophenone is introduced to solution to start a two-step reaction, which transforms the remaining NAD^+ into a fluorescent form. The second part of the reaction occurs after incubation with 100% formic acid, which stabilizes the reaction. The excitation wavelength and emission wavelength were 372 and 444 nanometers (nm), respectively. On figure 4, an overview of the reaction is presented. (Putt & Hergenrother, 2004; Venkannagari *et al.*, 2013)

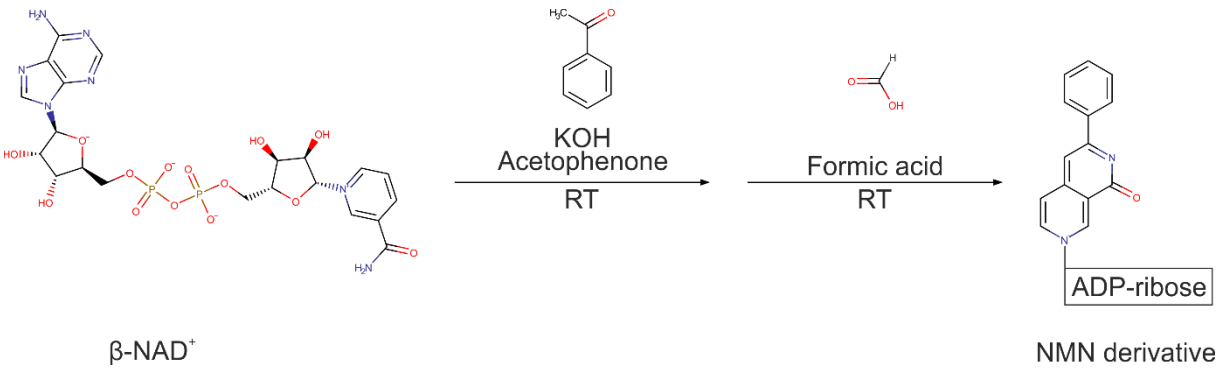

Figure 4: An overview of chemical conversion of NAD^+.

4.4 Cell cultures

To obtain Hela-, MDA-MB-231 –and MCF-7 –cells for further experiments, the cells were grown in an incubator with a temperature of +37 °C, CO_2 levels at 95% and O_2 levels at 5%. The cells were plated on 10 cm plates using Dulbecco's modified eagle's medium (DMEM; 10% volume/volume (V/V) fetal bovine serum (FBS), 1% (V/V) penicillin/streptomycin (P/S)) as growing medium. The cells were observed regularly, and they were divided into several plates when required. The cell lines were selected according to their reported ARTD10 expression levels. The breast cancer cell lines, MDA-MB-231 and MCF7, are suggested to express high amount of ARTD10, whereas HeLa cells, cervical cancer cells, are suggested to express only little as a compare thus serving as a negative control. (Cell atlas; Expression Atlas)

On table III, the overview of the PARP10 expression in the cell lines mentioned above is shown. The cells are arranged from highest expression levels to the lowest expression levels in transcripts per million (TPM) -units. The values were obtained from Cell Atlas and Expression Atlas.

Table III: An overview of TPM values of cell lines used in the experiment. The TPM values were obtained from Cell Atlas and Expression Atlas, and they differed from each other greatly. MCF7 cell line had several TPM values in Expression Atlas, the value on table is obtained from a comparative proteomic analysis of cell lines. At the time, TPM values for every cell line from both databases was unachievable. The Expression Atlas search was commenced with "PARP10", "*Homo sapiens*", "HeLa", "MDA-MB-231", and "MCF7". The bolded values were considered as expected values for the experiments. (Cell atlas; Expression Atlas)

PARP10 expression				
Cell line	**Cell line type**	**Organ (example)**	**Origin (example)**	**TPM (Cell Atlas/Expression Atlas)**
MCF7	Breast adenocarcinoma	Breast	Epithelial	**16.5**/2
MDA-MB-231	Breast ductal adenocarcinoma	Breast	Mammary gland	x/**15**
HeLa	Adenocarcinoma	Cervix	Epithelial	**6.6**/11

4.5 Cell confluency experiments with IncuCyte

The cell confluency experiments were done with MDA-MB-231 –and MCF7 –cells with IncuCyte. The IncuCyte is an incubator, which takes images of cells on clear 96-well plate in every two hours. The images are analyzed with IncuCyte ZOOM 2015A (IncuCyte), which analyses the total confluency of the cells, and thus, the viability. The obtained raw data is analyzed with any spreadsheet application, and the curves can be processed according to these values.

The quantity of the cells in each well of 96-well plates (Corning, 3599) were 50 000/ml, and the compounds used were dimethyl sulfoxide (DMSO), PARP10 inhibitor OUL35, topoisomerase II inhibitor Teniposide (VM-26, SML0609), potent topoisomerase I inhibitor Irinotecan hydrochloride (I1406), thymidylate synthase inhibitor 5-fluorouracil (5-FU) (F6627), anti-neoplastic ribonucleoside reductase hydroxyurea (HU) and DNA replication inhibitor Cytarabine (ARA-C) (C1768). (PubChem; Sigma-Aldrich)

Furthermore, the obtained data was processed with Excel (Microsoft), calculating the averages and standard error of the mean (SEM) values, and the curves were drawn using GraphPad Prism 8.0.2., and the curves were processed into their final form using CorelDRAW 2018 (Corel). On table IV, layout of the experiment is shown.

Table IV: Layout of the cell confluency experiment. All wells had a final volume of 200 µl.

	1	2	3	4	5	6	7	8	9	10	11	12
A	0.1 % DMSO	10 µM OUL35	0.1 % DMSO	0.1% DMSO	0.1 % DMSO	0.1% DMSO	0.1 % DMSO	10 µM OUL35	10 µM OUL35	10 µM OUL35	10 µM OUL35	10 µM OUL35
B												
C												
D												
E												
F			10 µM Teniposide	10 µM Irinotecan	10 µM 5-FU	100 µM HU	10 µM ARA-C	10 µM Teniposide	10 µM Irinotecan	10 µM 5-FU	100 µM HU	10 µM ARA-C
G												
H												

4.6 Cell fractionation

The cell treatments were performed as triplicates of all four set-ups (DMSO (control), OUL35, Hydroxyurea (+DMSO) and HU + OUL35), using 24 h -and 72 h time intervals. The cells were first counted, aim was to have 2 000 000 cells on each plate. The following day, the media was changed, and the compounds were added. On table V, the final concentrations of compounds are displayed.

Table V: Final concentrations of compounds on 10 cm plates. The stocks were 100% DMSO, 200 mM HU, and 10 mM OUL35.

Compound	Final concentration
DMSO	0.1%
HU	100 µM
OUL35	10 µM

The fractionation commenced with ice-cold 1x phosphate buffer serine (PBS) wash, followed by introduction of 500 µl of ice-cold fractionation buffer (20 mM HEPES, 10 mM KCl, 2 mM $MgCl_2$, 1 mM egtazic acid (EGTA), 1 mM ethylenediaminetetraacetic acid (EDTA), distilled water (dH_2O); added 1000x pefablock (1/5) and 1 mM TCEP just before pipetting). After the fractionation buffer was added on plates, the cells were scraped off, and lysate was pipetted into the 1.5 ml Eppendorf tube (700 µl/tube). The cells were then incubated on ice for 15 minutes.

After incubation, cells were passed through 27 G needle ten times, and centrifuged with microcentrifuge (Eppendorf centrifuge 5415 C; 10 minutes, 3000 rpm, +4 °C). After first centrifuge run, supernatant was transferred into separate 1.5 ml Eppendorf tube (cytoplasmic fraction). The obtained pellet was dissolved into 500 µl of fractionation buffer followed by ten passes of 25 G needle, and the suspension was centrifuged as mentioned previously.

After last centrifuging, supernatant was discarded, and the pellet was dissolved into 250 µl nuclear lysis buffer (tris buffer saline (TBS), 0.1% sodium dodecyl sulphate (SDS). Before freezing the fractions, the genome of nuclear fractions was sheared using water bath sonicator (Branson 3510) for approximately 10 seconds.

4.7 Western blot

Western blot is a method, which involves protein transfer from SDS-PAGE gel on a nitrocellulose or polyvinylidene fluoride (PVDF) membrane with electric field. The transfer can be made with dry, semi-dry or wet transferring (semi-dry was used in case of four membranes, and wet transfer in case of rest twelve membranes). In semi-dry western blot transfer method, the methanol in transfer buffer was replaced with ethanol (1x tris-glycine (TG) –buffer (BioRad), 20% ethanol (EtOH), dH_2O). After the transfer, membranes are incubated with blocking buffer (in this case; tris-buffered saline (TBS), 2% casein) to suppress nonspecific signals during imaging. The blocking is followed up by the immunostaining, which is usually a two-step incubation with primary antibodies and secondary antibodies. Both antibodies, primary and secondary, were diluted in blocking buffer. The primary antibody incubation occurs usually overnight, making sure as much antibodies as possible is bound to wanted protein. The horseradish peroxidase (HRP) labeled secondary antibodies bind to the primary antibodies and the enhanced chemiluminescence (ECL) provides luminescence when reacting with HRP and thus, visual bands. If the primary antibody is specific, only one protein band is visible after imaging. The imaging includes an ultraviolet (UV) exposure of blot, providing the luminescence mentioned previously.

A loading control should be made for band intensity determination. The determination is made via comparison between the wanted protein expression and expression level of highly expressed protein. The intensity can be determined with programs capable to sense the band intensities such as Image Lab (BioRad), and the value of wanted protein is divided by the loading control value. Before the loading control visualization, the membrane must be stripped from previous antibodies. To accomplish this, the membranes are firstly treated with warm stripping buffer (1x stripping buffer, 0.7% β-mercaptoethanol). Once the membrane is stripped from the antibodies from previous imaging, the membrane is washed and re-blocked. After re-blocking, the membrane can be blocked with new primary antibody.

Western blot analysis was performed to seek the amount of expressed PARP-10 in three different cell lines. These cell lines were HeLa, MDA-MB-231, and MCF7, from which HeLa had hypothetically lowest ARTD10 expression levels, MDA-MB-231 fair ARTD10 expression levels, and MCF7 having hypothetically the highest ARTD10 expression levels of the

experiment. The primary antibody used was ARTD10 antibody from Santa Cruz Biotechnology (5H11, unconjugated monoclonal rat IgG, 1/200 dilution) and the secondary antibody used was goat-anti-rat from Jackson (112-035-003, HRP conjugated polyclonal goat IgG, 1/5000 dilution). The loading control for cytoplasmic fractions was performed with β-tubulin antibody from Jackson (ab21058, HRP conjugated polyclonal rabbit IgG, 1/1000 dilution), and in case of nuclear fractions, Histone H3 from Novus (NB500-171, unconjugated polyclonal rabbit IgG, 1/2000 dilution) was used and as a secondary antibody, goat-anti-rabbit from Jackson (111-035-003, HRP conjugated polyclonal goat IgG, 1/5000 dilution). The bands were visualized with ECL (Advansta WesternBright™).

5. Results and discussion

5.1 Protein purification

ARTD10 was purified with IMAC, heparin, AEC, and SEC, and on following images, the level of purity after each chromatography step is represented. This step was made to obtain as pure ARTD10 as possible. Overall, the purity level of ARTD10 solution was appropriate for biochemical analysis after SEC, and as expected, the first steps (IMAC, heparan, AEC) did not purify the protein solution to its final form. In the end, ARTD10 concentration of approximately 35.90 μM (3.95 mg/ml) and yield of 2.63 mg/l was obtained.

On figure 5, a purity check with SDS-PAGE of ARTD10 after IMAC is shown. As expected, impure protein solution after the first step of the purification was obtained. This image also includes the gels with IMAC elution, and heparan flow-through. On figure 6, the purity level of the protein solution containing ARTD10 after AEC run is shown alongside the chromatogram. According to the peaks of AEC chromatogram, fractions 2, 9, 13, and 21 were collected, to see whether ARTD10 is present or not. On figure 7, the SDS-PAGE check of ARTD10 purity after SEC run alongside chromatogram is shown. According to SEC chromatogram, fractions 9, 13, 17, and 21 were collected. Furthermore, fractions 12-20 were combined for purity check. These fractions were chosen to see whether there is ARTD10 present or not. The standard well was contaminated with protein samples from other wells. Thus, it is not shown on figure 7.

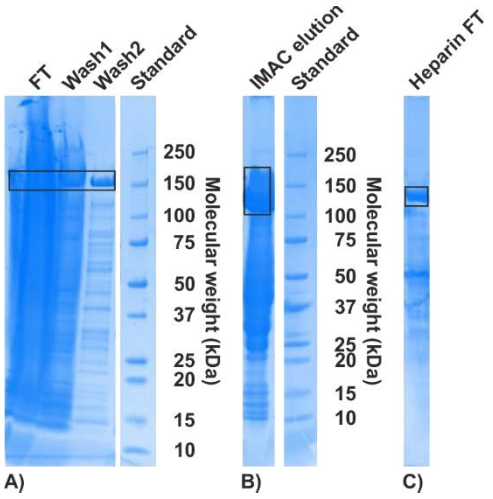

Figure 5: Gel images of ARTD10 purity after IMAC and heparin (three separate gels). A and B represents two separate gels containing IMAC samples, whereas C represents a gel with ARTD10 solution after heparin run. A contains the flow-through, wash with Washing Buffer 1 and wash with Washing Buffer 2, B contains the flow-through with elution buffer, and C contains heparan flow-through with buffer A. The bands representing ARTD10 are marked with a rectangle.

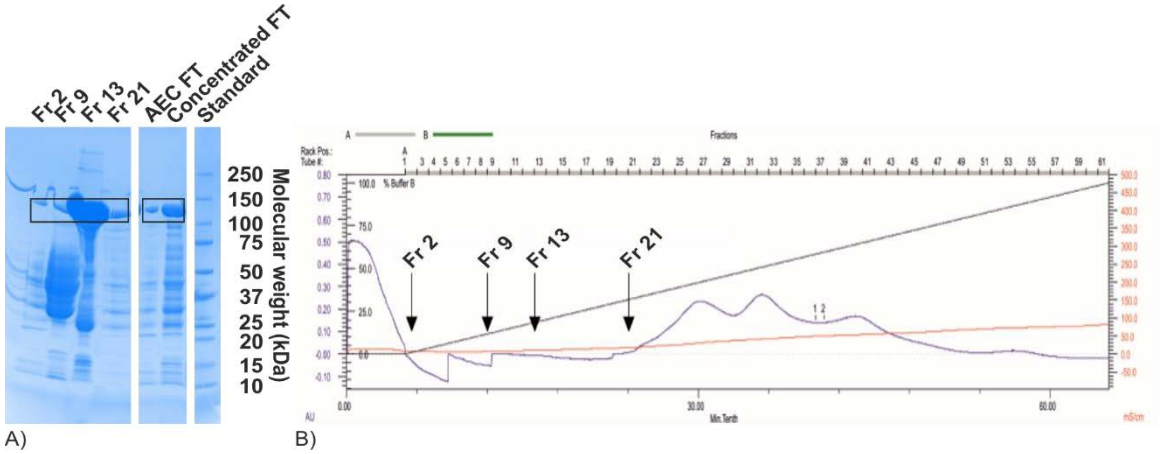

Figure 6: A gel image and AEC chromatogram. A represents the gel image showing level of ARTD10 purity after the chromatography run, and the bands representing ARTD10 are marked with rectangle. The bands consist of AEC run (fractions 2, 9, 13 and 21), and concentrated elution of AEC, as comparison for AEC elution. B represents the AEC chromatogram.

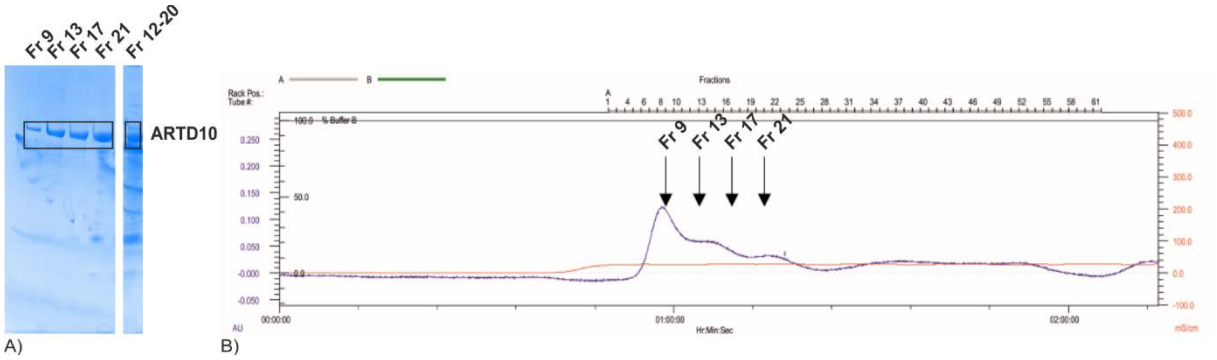

Figure 7: A gel image and SEC chromatogram. A represents the SDS-PAGE gel run after SEC run, and the bands representing ARTD10 are marked with rectangle. The gel image consists of Fraction 9, 13, 17, 21, and fraction combination (12-20). B represents SEC chromatogram for ARTD10, from which the fractions for purity check were chosen.

5.2 IC_{50}

According to previous studies, the construct of ARTD has most likely an effect on the inhibition. To verify that whether OUL35 is equally effective against full-length ARTD10 and the catalytic domain or not, IC_{50} experiment was made. Thorsell and colleagues (2017) recognized that the enzymatic activity of catalytic domain of ARTD1, ARTD2, and ARTD3 is significantly decreased as compared to the full-length construct, whereas ARTD10 activity did not vary. Venkannagari and colleagues (2016) has measured the IC_{50} value of catalytic domain of ARTD10 with OUL35 as 329 nM ($pIC_{50} \pm$ SEM: 6.48 ± 0.04), whereas an average IC_{50} value of three experiments was 510 nM ($pIC_{50} \pm$ SEM: 6.29 ± 0.04). Thus, it can be concluded that the full-length ARTD10 inhibition with OUL35 lowers the activity at same level as catalytic domain, indicating there is no large differences between the constructs. On figure 8, a curve representing the ARTD10 activity with presence of OUL35 with different concentrations is shown. (Venkannagari *et al.*, 2016; Thorsell *et al.*, 2017)

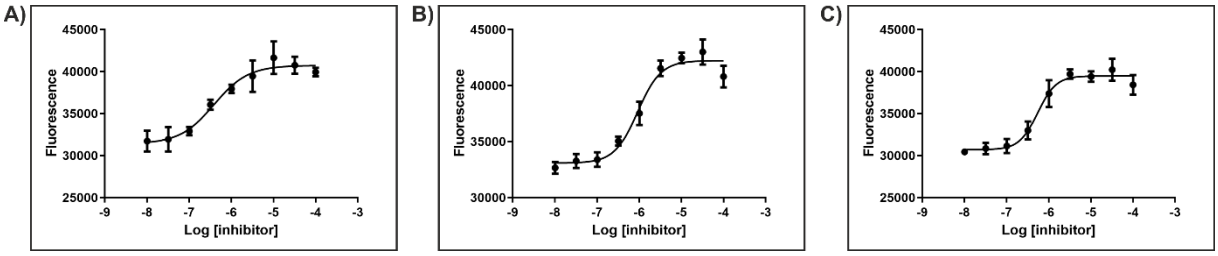

Figure 8: IC_{50} curves. The IC_{50} value was 510 nM (pIC_{50} ± SEM: 6.29 ± 0.04).

These results support the spotted inhibitory effect from cell experiments. The IC_{50} value of full-length ARTD10 is close to the IC_{50} value obtained from a catalytic domain. There is, however, a small difference on these results, suggesting the other domains may have an influence on the catalytic activity. However, as the differences are minimal, either the full-length protein or catalytic fragment can be used likely in reliable IC_{50} measurements and ranking of the inhibiting compounds. (Venkannagari *et al.*, 2016; Thorsell *et al.*, 2017)

5.3 ARTD10 localization and inhibitor effects on expression levels

This experiment was conducted to detect whether OUL35 has effect on ARTD10 localization in cells under DNA stress. To obtain the results, the cells were treated as explained earlier in sections 4.6 and 4.7. On figures 9 and 10, the western blot images representing the results of OUL35 effects on different cell lines are shown in nucleus and cytoplasm. On figure 9, only the bands are shown due lack of loading control, whereas on figure 10, the images are combined with a graph representing the band intensity level against amount of β-tubulin. The alphabets A-H represent the different membranes, being in case of figure 9, nuclear fractions, and in case of figure 10, a comparison of amount of cytoplasmic ARTD10 after 24h and 72h. A and B represents the comparison of overall ARTD10 between the cell lines used in the experiment, C-D being comparison of amount of ARTD10 between DMSO (control), OUL35, HU and HU with OUL35 in HeLa cell fractions, E-F being comparison of amount of ARTD10 between DMSO (control), OUL35, HU and HU with OUL35 in MDA-MB-231 cells, and G-H being comparison of amount of ARTD10 between DMSO (control), OUL35, HU and HU with OUL35 in MCF7 cell fractions. The cells were treated on images A-B with 0.1% DMSO, and

on images C-H, with 0.1% DMSO, 10 µM OUL35, DMSO and 20 µM HU, and OUL35 and HU. Examples of western blot images are shown in appendix.

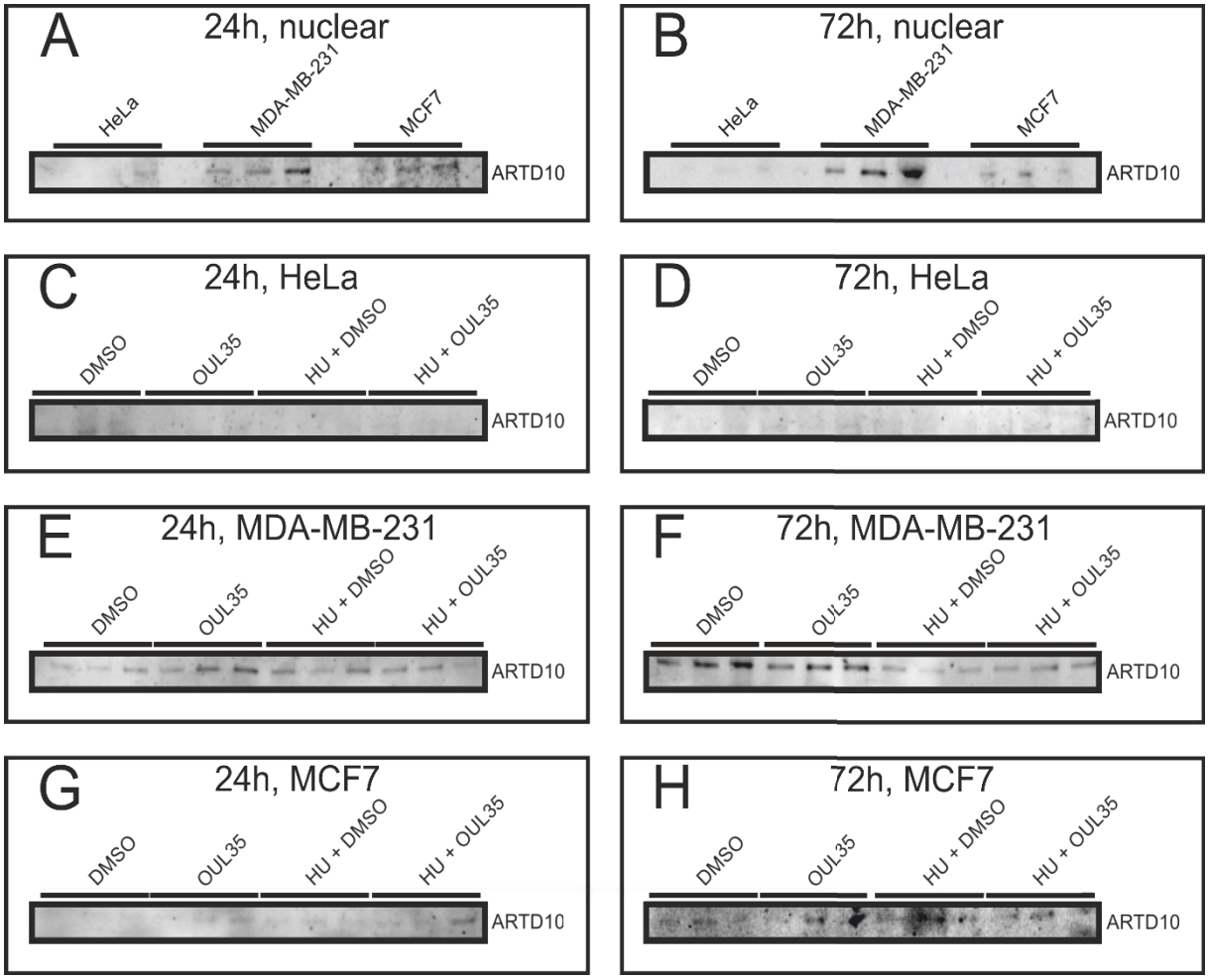

Figure 9: ARTD10 expression levels in nucleus. A and B represents the ARTD10 expression levels in HeLa, MDA-MB-231 -and MCF7 cell-lines with 0.1% DMSO treatment, C and D represents ARTD10 expression levels in nuclear fractions of HeLa cells, E and F represents ARTD10 expression levels in nuclear fractions of MDA-MB-231 cells, and G and H represents ARTD10 expression levels in nuclear fractions of MCF7 cells. All cell lines were treated for 24h and 72h, respectively.

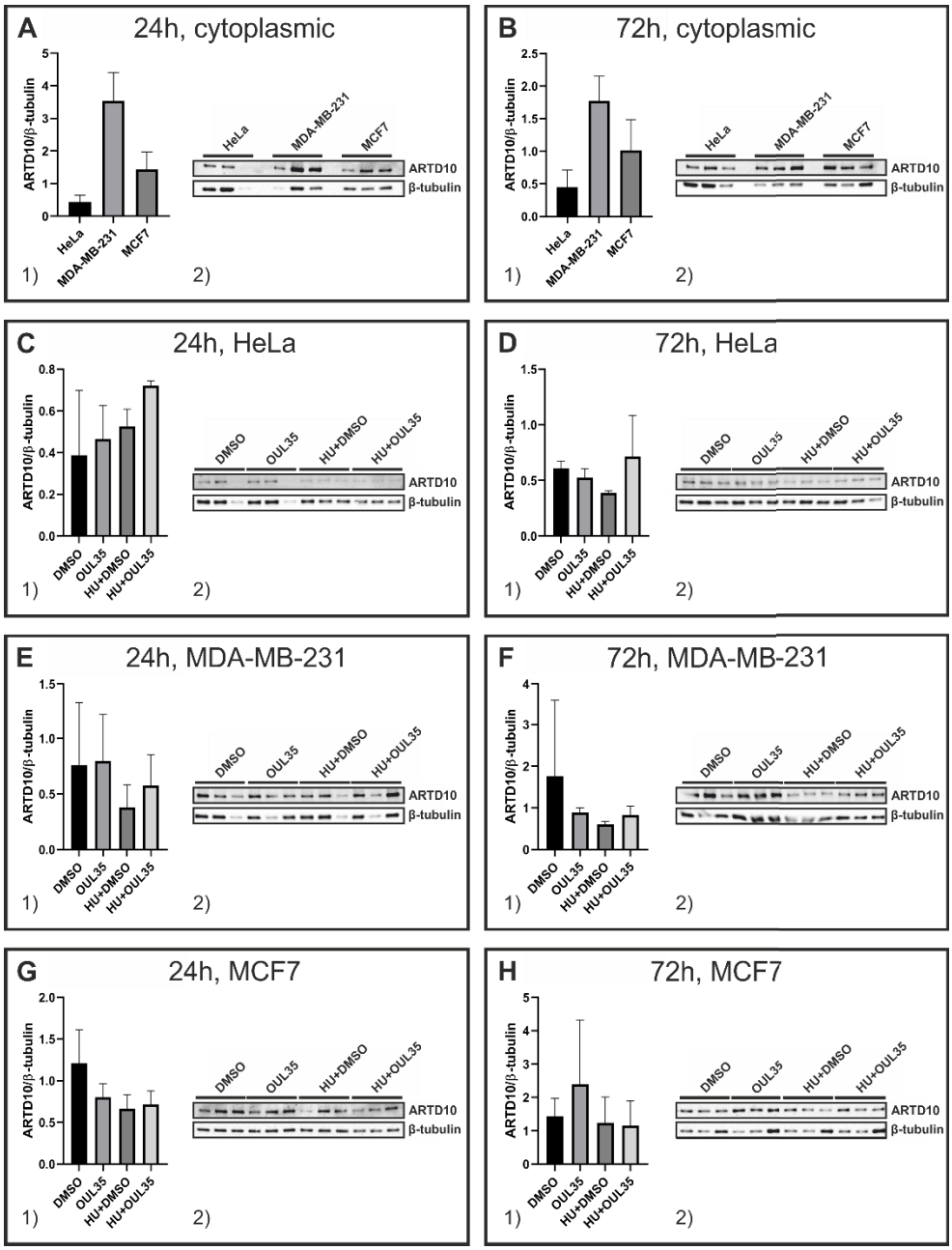

Figure 10: ARTD10 expression levels in cytoplasmic samples. A and B represents expression levels in HeLa, MDA-MB-231 -and MCF7 cell-lines with 0.1% DMSO treatment, C and D represents ARTD10 expression levels in cytoplasmic fractions of HeLa cells, E and F represents ARTD10 expression levels in cytoplasmic fractions of MDA-MB-231 cells, and G and H represents ARTD10 expression levels in cytoplasmic fractions of MCF7 cells. All cell lines were treated for 24 h and 72 h, respectively.1 represents the graph displaying the band intensity, whereas 2 represents the ARTD10-bands from western blot.

According to the band intensities, such as images G and H on figure 10, the ARTD10 levels in cytoplasm appears to decrease after 24h. Also, OUL35 appear to have no effect on cytoplasmic ARTD10. In the nucleus, there appear to be less ARTD10 after treating the cells with compounds as compared to the DMSO (control). However, the triplicates from this experiment are not equal (figures 9 and 10), therefore the consistency should be improved. The main improvements are elimination of pipetting errors and collecting equal amounts of cells from plates. Furthermore, because of the inappropriate secondary antibody for loading control of nuclear fractions, the ARTD10 level quantification in nucleus was unachievable. Thus, this experiment should be made again, and in case of nuclear fractions, with different antibodies. The used antibody was anti-H3, hence, and another antibody for this experiment could be against H4 histone. Alternatively, the fractions could be analyzed with protein amount determination before SDS-PAGE using protein concentration measuring devices such as NanoDrop, to have a backup, even if the loading control is insufficient. Moreover, the results don't indicate HU effect in translocation of ARTD10 from cytoplasm into nucleus, hence, more experiments should be conducted.

Alongside the localization results, the results show that the MDA-MB-231 cells expresses more ARTD10 than the other cell lines used in the experiment, as seen on images A and B (figure 10). MCF7 cells appears to express more ARTD10 than HeLa cells despite the search result from Expression Atlas, and MCF7 expresses clearly less ARTD10 than MDA-MB-231 cells, unlike Cell Atlas informed. Therefore, the values from databases should not blindly be relied on. The results from the localization experiments indicates that at 24h, the treatment with OUL35 has no drastic effect on ARTD10 levels on cytoplasm as compared to control (DMSO treatment), as seen on figures C-H (figure 10). Also, HU alone appear to increase the amount of cytoplasmic ARTD10 slightly, indicating this compound induces ARTD10 expression, and according to the graphics, OUL35 seem to enhance this effect, as represented on images C1, D1, and E1.

5.4 Sensitization effect of ARTD10 inhibition

To determine whether OUL35 sensitizes breast cancer cell lines (MCF7, MDA-MB-231) to DNA damage, the IncuCyte observation was conducted as described in section 4.5. During this experiment, the cells were treated with teniposide, irinotecan, 5-FU, HU, and ARA-C. OUL35 acted as a sensitization compound, and DMSO as a control. DMSO is used broadly as a solvent in topological treatments as penetration increaser, cell cryopreservation, and pharmacology and toxicology. It has been noted to possess medical properties such as muscle relaxation, diuretics, anti-inflammation, vasodilation, and nerve blockade (Verheijen *et al.*, 2019). OUL35 is used as a selective ARTD10 inhibitor. It binds to the NAD^+ pocket of ARTD10, preventing the MARylation. According to the results, the single-agent effect of OUL35 had no effect on cellular proliferation, whereas Venkannagari and colleagues (2016) noticed this compound to preserve HeLa cells, via inhibiting the apoptosis due overexpression of ARTD10. It appears ARTD10 inhibition has a dual effect, both sensitizing to DNA damage, and protecting from apoptosis. (Venkannagari *et al.*, 2016)

Hydroxyurea (HU) is a potent teratogen with anticancer properties. It inhibits ribonucleotide reductase, which takes part in deoxynucleoside triphosphate (dNTP) synthesis. When dNTP synthesis is inhibited, DNA synthesis is prevented and the early S phase cell cycle is halted (Benito *et al.*, 2007). One result from a study of Montano and colleagues (2012) showed that 1 mM concentration decreases MDA-MB-231 cell viability approximately to 50%. In case of MCF7 cells, viability is proven to be decreased by HU from concentrations 10-625 μM, and to kill these cells effectively, concentration should be over 1 mM. (Montano *et al.*, 2012; Shahabi *et al.*, 2014).

Teniposide is used as an anticancer drug, primarily in case of acute lymphocytic leukemia of children, brain tumors and lung cancer. This compound acts as an inhibitor of mitosis, by stabilizing topoisomerase II (Yoneda & Cross, 2010). Sánchez-Alcázar and colleagues noted teniposide to increase cytochrome c expression in mitochondria of MDA-MB-231 cells, resulting in lower oxygen intake (Sánchez-Alcázar *et al.*, 2001).

Irinotecan hydrochloride is used as a chemotherapeutic, which was first used as a treatment for colorectal cancer (CRC). It is a prodrug, which is metabolized into its active form, 7-ethyl-10-hydroxycampothecin (SN-38), by carboxylesterase. This compound is one of the camptothecins

(CPTs), which targets specifically topoisomerase I. The cytotoxic effects of CPTs are specified for S-phase (Rasheed & Rubin, 2003; Fujita *et al.*, 2015).

5-fluorouracil (5-FU) is commonly used as treatment in case of CRC. The cytotoxicity of this compound is based on DNA damage caused via fusing into DNA, thymidylate synthase (TS) inhibition by 5-fluoro-2´-deoxyuridine-5´-monophosphate (FdUMP, a 5-FU metabolite) followed by DNA and thymidylate biosynthesis inhibition, and fusion of 5-FU into RNA followed by RNA processing and function alterations (Copur *et al.*, 1995). Li and colleagues noted 53BP1 has a synergetic effect with 5-FU against MDA-MB-231 -and MCF7 cells (Li *et al.*, 2013). It has been detected 5-FU cytotoxic effects on both MDA-MB-231 -and MCF7 cells are visible, if the concentration is exceeded 100 µM (Gomaa *et al.*, 2015; Chen *et al.*, 2017).

Cytarabine (ARA-C) is a potent drug against acute myeloid leukemia. It inhibits the DNA during checkpoint of G1/S phase, and in case of some leukemic cells, prevents progression into S-phase (Momparler, 2013). In previous studies, both MDA-MB-231 -and MCF7 cells are noticed to be sensitive to this compound (Strasser *et al.*, 2006; Li *et al.*, 2008).

5.4.1 Example specimens of visual effects of potent and ineffective compounds

On figures 11 and 12, the cell viability at day 7 of the experiment are shown. Figure 11 represents the observation of MDA-MB-231 whereas figure 12 the observation of MCF7 cells. On these images, cells are under conditions of DMSO, OUL35, HU with and without OUL35, and irinotecan with and without OUL35. The images are labeled as letters A-F, A being 0.1% DMSO-treated cells, B being 10 µM OUL35-treated cells, C being 100 µM HU treated cells with 0.1% DMSO, D being 100 µM HU with 10 µM OUL35, E being 10 µM irinotecan with 0.1% DMSO, and F being 10 µM irinotecan with 10 µM OUL35.

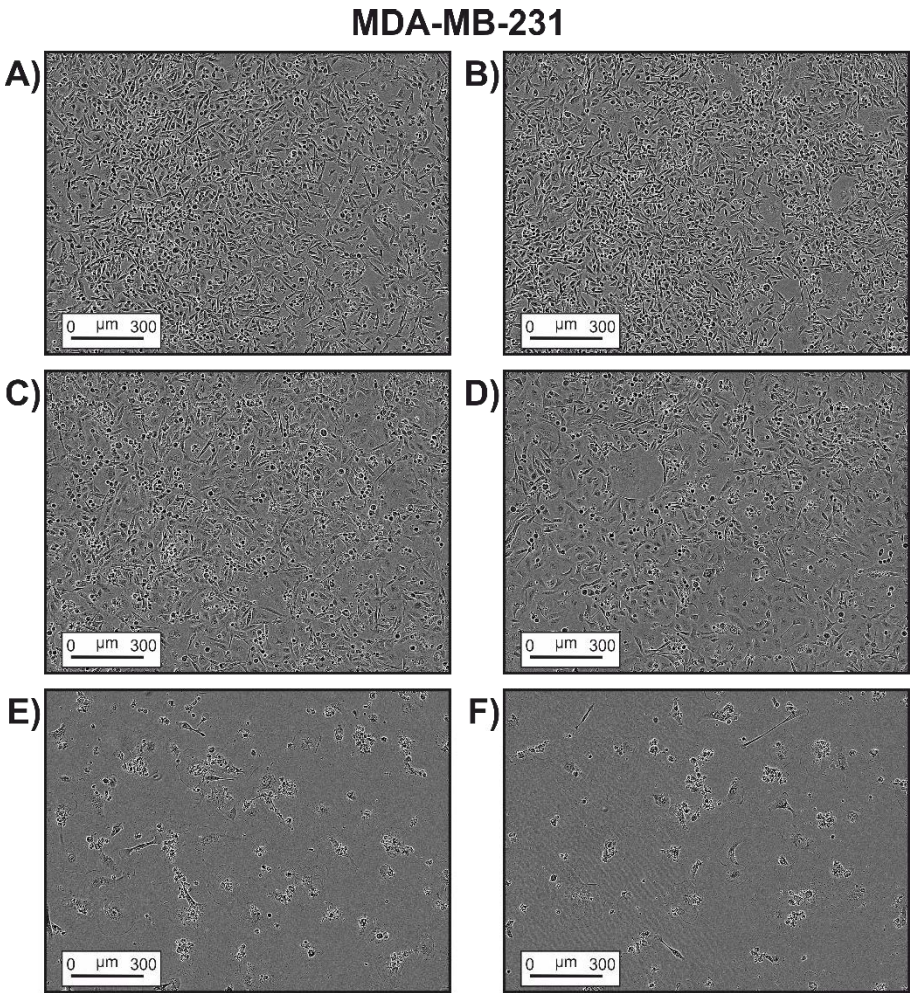

Figure 11: MDA-MB-231 cells, day 7 of the observation. A represents MDA-MB-231 cells with DMSO treatment, B represents MDA-MB-231 cells with OUL35 treatment, C represents MDA-MB-231 cells with HU treatment, represents MDA-MB-231 cells with HU and OUL35 treatment, E represents MDA-MB-231 cells with irinotecan treatment, and F represents MDA-MB-231 cells with irinotecan and OUL35 treatment.

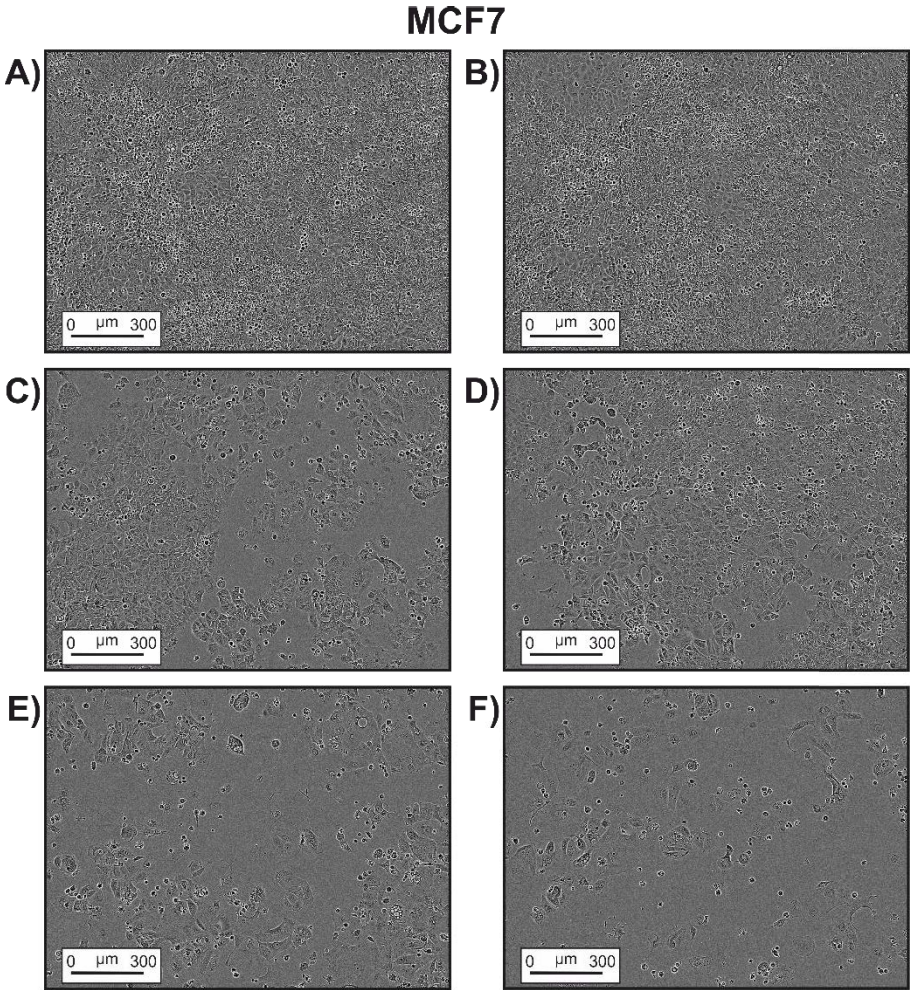

Figure 12: MCF7 cells, day 7 of the observation. A represents MCF7 cells with DMSO treatment, B represents MCF7 cells with OUL35 treatment, C represents MCF7 cells with HU treatment, represents MCF7 cells with HU and OUL35 treatment, E represents MCF7 cells with irinotecan treatment, and F represents MCF7 cells with irinotecan and OUL35 treatment.

As seen on figures 11 and 12, both cell lines are undoubtedly dying under conditions of irinotecan, and the OUL35 barely enhance this effect, as on images E and F on both figures. As a comparison, DMSO, OUL35 only, and HU with and without OUL35 appears to inflict no or only little damage to the cells, as shown on images C and D on both figures.

5.4.2 Graphical representations of IncuCyte experiment

On figure 13, the combined curves for IncuCyte observations can be seen. The backbone of the curves consists of values obtained from average confluency from three plates. The alphabets A-E represents the different setups. A indicates teniposide treatment, B irinotecan treatment, C 5-FU treatment, D HU treatment, and E ARA-C treatment. Numerals 1 and 2 represents the cell lines, 1 indicating MDA-MB-231, whereas 2 indicates MCF7 cells.

According to the graphs, HU kills MDA-MB-231 cells slightly more effectively than teniposide, whereas MCF7 cells appear to suffer as much damage as with teniposide treatment (figures 13A and 13D). On the last curves, the results indicate that ARA-C is almost as effective as irinotecan, and OUL35 enhances the cytotoxic effects on MCF7 cells (figure 13E). It appears that the irinotecan and ARA-C are the most potent cytotoxic compounds for the cells used in this experiment, as shown on figures 13B and 13E. The least cytotoxic compounds to MDA-MB-231 -and MCF7 cells are teniposide, 5-FU and HU, as figures 13C and 13D represents.

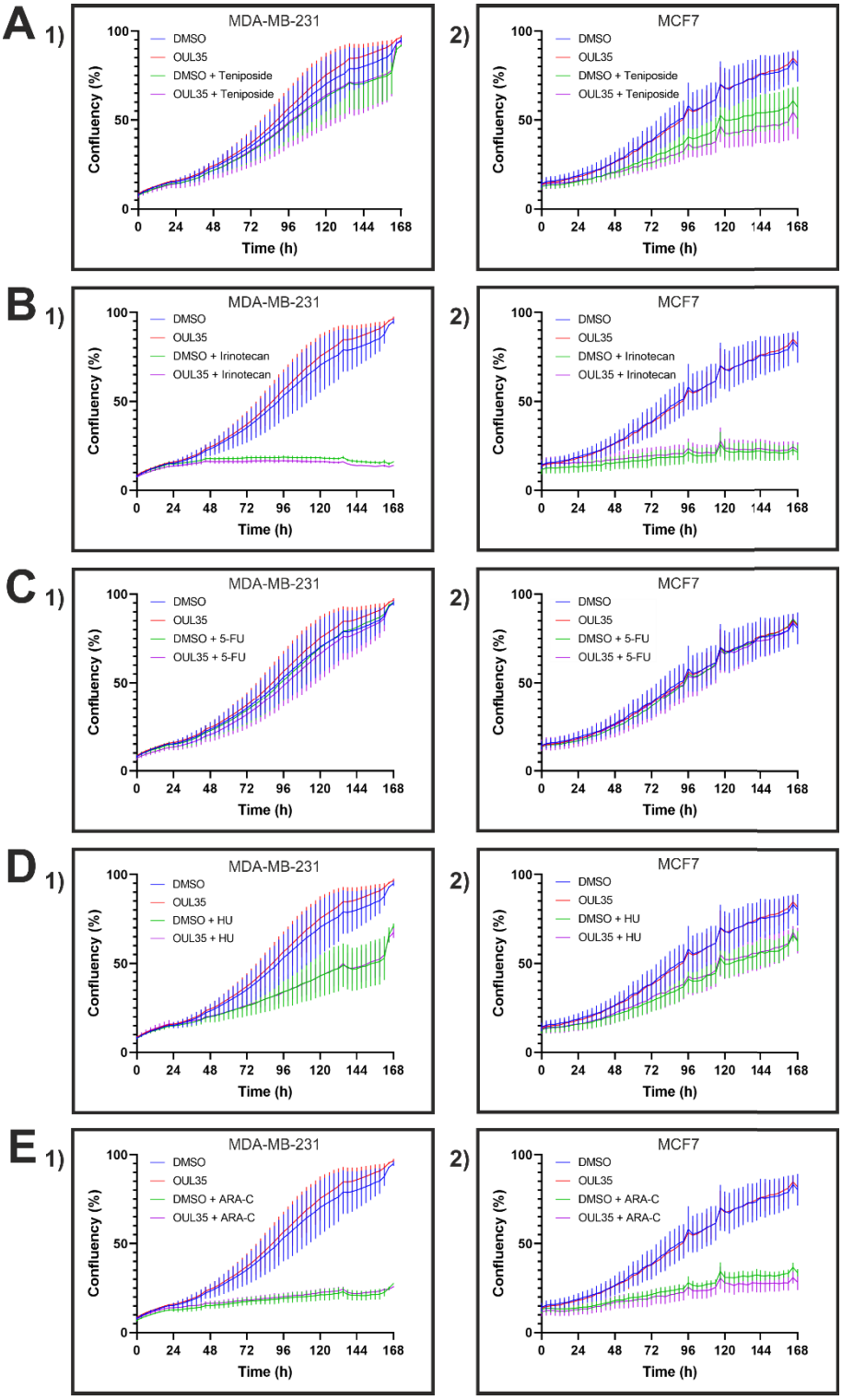

Figure 13: Graphs representing the cell confluences during IncuCyte observation. A represents the Teniposide-treated cells, B represents the Irinotecan treatment, C represents 5-FU treatment on cells, D represents HU treatment on cells, and E represents ARA-C treatment on cells. The numeral 1 represents MDA-MB-231 cells and 2 represents MCF7 cells.

5.4.3 The compounds with the least cytotoxic effect on the cells

According to the results, HU alone has a slight impact on MDA-MB-231 cells, and OUL35 appear to increase this effect, as represented on curve D1 (figure 13). Whereas in case of MCF7 cells this compound expressed only a little cytotoxic activity, and OUL35 had only a slight effect on cytotoxicity of this compound, as shown on curve D2 (figure 13). Teniposide appears to have only a slight cytotoxic impact on MDA-MB-231 -and MCF7 cells. At the used concentration, OUL35 appeared to protect MDA-MB-231 cells, possibly due inhibition of ARTD10-induced apoptosis, whereas showing a slight impact on MCF7 cells (Venkannagari *et al.*, 2016). Hence, it can be concluded that OUL35 is not the best synergetic compound for teniposide. These events can be seen on curves A1 and A2 (figure 13). The last least effective compound to be analyzed is 5-FU. According to the results, MDA-MB-231 cell viability appear to decrease a little, and OUL35 appear to show a slight cell preservation, as shown on curve C1 (figure 13). Furthermore, in case of MCF7 cells, this compound has no effect, and it appears the OUL35 increase the cell viability slightly, as illustrated on the curve C2 (figure 13).

5.4.4 The compounds with the most cytotoxic effect on the cells

Native MDA-MB-231 -and MCF7 cells are detected to be sensitive to SN-38 (Jandu *et al.*, 2016), and according to the obtained results, this compound appears to have a clear cytotoxic effect on these cell lines. However, the cytotoxic effect of this compound was excessive, indicating lower concentration should have been used. The OUL35 was not enhancing the cytotoxic effects significantly, and if the concentration is increased, irinotecan is so toxic the sensitization results are difficult to verify. The powerful cytotoxic effects of irinotecan are visualized on curves B1 and B2 (figure 13). Alongside irinotecan, ARA-C was most effective compound. OUL35 had only a slight effect on the cytotoxicity, decreasing viability of MDA-MB-231, as visualized on curve E1 (figure 13), and increasing MCF7 viability a little, as curve E2 (figure 13) indicates.

5.4.5 Statistical significance of the cell viability results

To determine the statistical significance of the cell confluency curves from IncuCyte experiment, a one-way analysis of variance (ANOVA) test was conducted, and the graphics obtained from this test is shown on figure 14. The values represented as a graph are averages of last time point and SEM value, and above each graph, statistical significance is shown (ns stands for not significant, ** stands for $p < 0.005$, *** stands for $p < 0.001$, and **** stands for $p < 0.0001$). According to the obtained results, it can be indicated that OUL35 does not affect significantly on the cellular proliferation on neither MDA-MB-231 nor MCF7 cells. Also, the OUL35 does not enhance the effect of any compound significantly. Teniposide has only a slight cytotoxic effect on both cell lines, indicating the too low concentration. In the stark contrast, irinotecan kills cells too effectively, leaving only approximately 20% of the cells alive at the end of the observation, indicating too high concentration used in the experiment. 5-FU was the least cytotoxic compound used during the experiment, suggesting too low concentration was used. HU in the other hand was killing roughly half of the cells during the observation period, having less effect on the MCF7 cells. Alongside irinotecan, ARA-C kills cells from both cell lines effectively, indicating the too high concentration in the experiment.

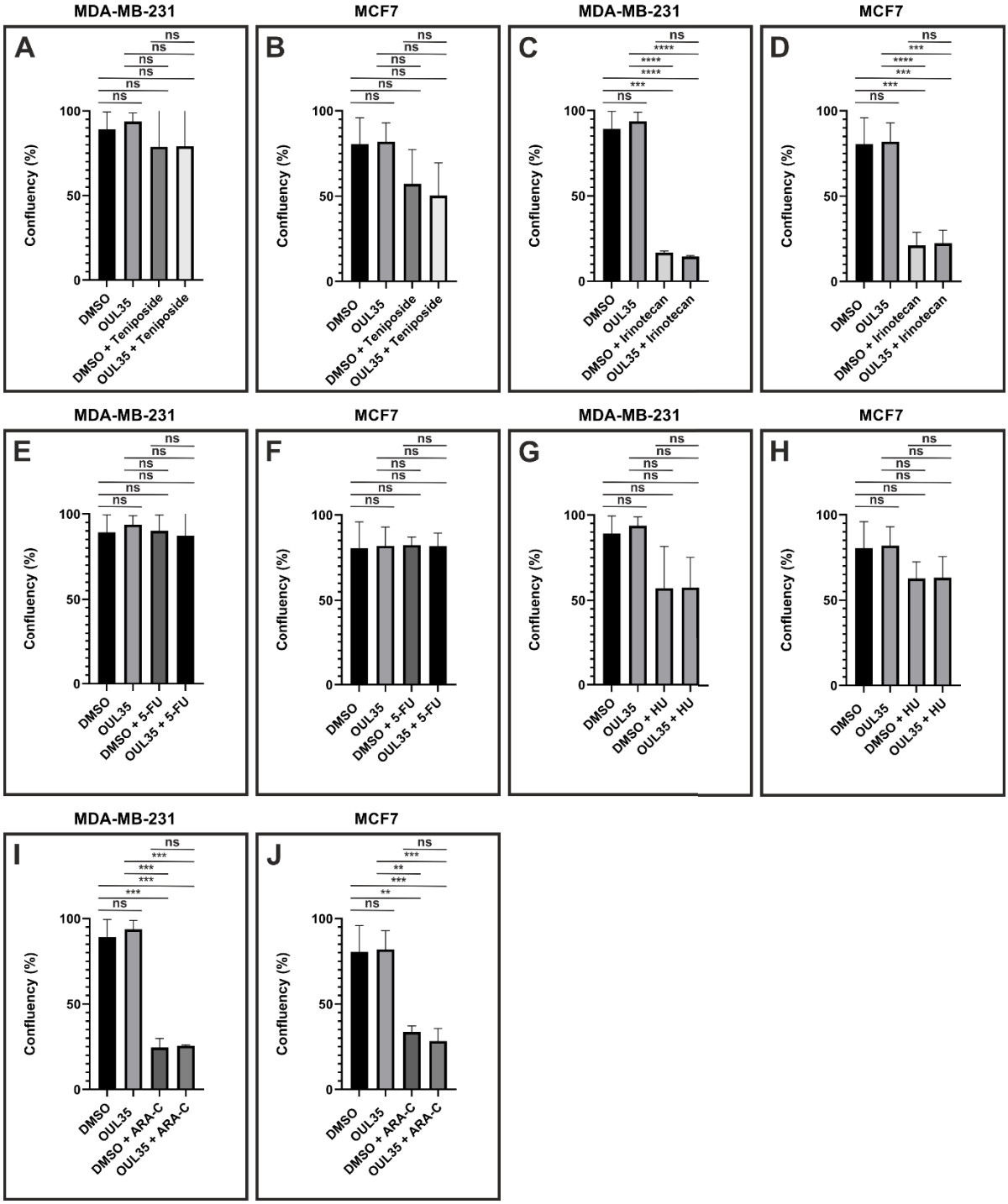

Figure 14: A one-way ANOVA test. Alphabets A-D represents the MDA-MB-231 -and MCF7 cells with different treatments. A and B represents MDA-MB-231 cells and MCF7 cells with teniposide treatment, whereas C and D represents MDA-MB-231 cells and MCF7 cells with irinotecan treatment, E and F represents MDA-MB-231 cells and MCF7 cells with 5-FU treatment, G and H represents MDA-MB-231 cells and MCF7 cells with HU treatment, and I and J represents MDA-MB-231 cells and MCF7 cells with ARA-C treatments.

5.4.6 Summary of the cell sensitization

As a summary, according to the one-way ANOVA test, the only compounds with statistically significant results were irinotecan, as proven on graphs C and D and ARA-C, as shown on graphs I and J (figure 14). According to these results, it can be concluded that these compounds had most likely too high concentrations. The OUL35 did not enhance significantly the cytotoxic effects of any compounds used during the experiment, suggesting there should be more cell lines to be tested. The least effective compound was 5-FU, which had no effect on neither cell lines, suggesting the used concentration was too low. This can be seen on graphs C1 and C2 (figure13), and graphs E and F (figure 14).

5.5 Future and the next steps

In the future, the cell confluency studies could be made with broader variety of cell lines alongside different compounds, such as cisplatin, irinotecan and ARA-C with lower concentrations, 5-FU and teniposide with higher concentration, and doxorubicin. These compounds should be tested alongside different ARTD10 inhibitors with varying concentrations, to seek the most appropriate combinations. Another appropriate option is to use immunostaining to detect the localization more efficiently, which was planned but not established due to challenges on finding appropriate antibody within already tight time schedule. Furthermore, the DNA-damaging agent/PARPi combinations should be tested with native cells alongside cancer cells, such as MDA-MB-231, to seek the concentrations killing only the cancer cells. The mechanism changing the ARTD10 levels after treatment of different DNA-damaging agents, such as irinotecan with and without OUL35, could be quantified using western blot assay.

6. Conclusions

According to the results obtained from this experiment, it can be concluded the full-length ARTD10 inhibition does not vary from the catalytic domain, OUL35 may enhance the effect of DNA damaging agents, and there is a possibility that HU might have an influence on nuclear translocation of ARTD10. However, in case of sensitization -and translocation studies, the effects of these compounds are cell line dependent, and the statistical significance is not occurring with successive rate. Thus, the obtained results warrant larger studies using a wider range of breast cancer cell lines alongside MDA-MB-231 -and MCF7 cells, such as T-47D, and other DNA damaging agents, such as cisplatin, alongside OUL35. Furthermore, the discovery of ARTD10 subtypes and sensitizing mutations in cancer could lead to insights to be utilized in clinical studies.

7. References

Bartlett E, Bonfiglio JJ, Prokhorova E, Colby T, Zobel F, Ahel I, Matic I (2018) Interplay of Histone Marks with Serine ADP-Ribosylation. Cell Reports, 24, 3488-3502.e5. 10.1016/j.celrep.2018.08.092.

Benito JM, López M, Lozano S, Ballesteros C, González-Lahoz J, Soriano V (2007) Hydroxyurea exerts an anti-proliferative effect on T cells but has no direct impact on cellular activation. Clinical and Experimental Immunology, 149, 171–177. 10.1111/j.1365-2249.2007.03412.x.

Berti PJ, Blanke SR, Schramm VL (1997) Transition State Structure for the Hydrolysis of NAD+ Catalyzed by Diphtheria Toxin. Journal of the American Chemical Society, 119, 12079–12088. 10.1021/ja971317a.

Bian C, Zhang C, Luo T, Vyas A, Chen S-H, Liu C, Kassab MA, Yang Y, Kong M, Yu X (2019) NADP+ is an endogenous PARP inhibitor in DNA damage response and tumor suppression. Nature Communications. 10, 10.1038/s41467-019-08530-5.

Bock FJ, Todorova TT, Chang P (2015) RNA Regulation by Poly(ADP-Ribose) Polymerases. Molecular Cell, 58, 959–969. 10.1016/j.molcel.2015.01.037.

Bruijnincx PCA, Sadler PJ (2008) 'New Trends for Metal Complexes with Anticancer Activity'. Current opinion in chemical biology, 12, 197–206. 10.1016/j.cbpa.2007.11.013.

Bütepage M, Eckei L, Verheugd P, Lüscher B (2015) Intracellular Mono-ADP-Ribosylation in Signaling and Disease. Cells, 4, 569–595. 10.3390/cells4040569.

Camero S, Ceccarelli S, De Felice F, Marampon F, Mannarino O, Camicia L, Vescarelli E, Pontecorvi P, Pizer B, Shukla R, Schiavetti A, Mollace MG, Pizzuti A, Tombolini V, Marchese C, Megiorni F, Dominici C (2019) PARP inhibitors affect growth, survival and radiation susceptibility of human alveolar and embryonal rhabdomyosarcoma cell lines. Journal of Cancer Research and Clinical Oncology, 145, 137–152. 10.1007/s00432-018-2774-6.

Chen Q, Kassab MA, Dantzer F, Yu X (2018) PARP2 mediates branched poly ADP-ribosylation in response to DNA damage. Nature Communications, 9, 3233. 10.1038/s41467-018-05588-5.

Chen X-X, Leung GP-H, Zhang Z-J, Xiao J-B, Lao L-X, Feng F, Mak JC-W, Wang Y, Sze SC-W, Zhang KY-B (2017) Proanthocyanidins from Uncaria rhynchophylla induced apoptosis in MDA-MB-231 breast cancer cells while enhancing cytotoxic effects of 5-fluorouracil. Food and Chemical Toxicology, 107, 248–260. 10.1016/j.fct.2017.07.012.

Cheung-Ong K, Giaever G, Nislow C (2013) DNA-Damaging Agents in Cancer Chemotherapy: Serendipity and Chemical Biology. Chemistry & Biology, 20, 648–659. 10.1016/j.chembiol.2013.04.007.

Copur S, Aiba K, Drake JC, Allegra CJ, Chu E (1995) Thymidylate synthase gene amplification in human colon cancer cell lines resistant to 5-fluorouracil. Biochemical Pharmacology, 49, 1419–1426. 10.1016/0006-2952(95)00067-A.

Curtin N, Szabo C (2013) Therapeutic Applications of PARP Inhibitors: Anticancer Therapy and Beyond. Molecular aspects of medicine. 34, 10.1016/j.mam.2013.01.006.

Dabin J, Fortuny A, Polo SE (2016) Epigenome Maintenance in Response to DNA Damage. Molecular Cell, 62, 712–727. 10.1016/j.molcel.2016.04.006.

D'Amours D, Desnoyers S, D'Silva I, Poirier GG (1999): Poly(ADP-ribosyl)ation reactions in the regulation of nuclear functions. Biochemical Journal, 342, 249–268. 10.1042/bj3420249

Dawicki-McKenna JM, Langelier M-F, DeNizio JE, Riccio AA, Cao CD, Karch KR, McCauley M, Steffen JD, Black BE, Pascal JM (2015) PARP-1 activation requires local unfolding of an autoinhibitory domain. Molecular cell, 60, 755–768. 10.1016/j.molcel.2015.10.013.

Dockery L, Gunderson C, Moore K (2017) Rucaparib: the past, present, and future of a newly approved PARP inhibitor for ovarian cancer. OncoTargets and therapy. 10, 3029–3037. 10.2147/OTT.S114714.

Ekblad T, Lindgren AEG, Andersson CD, Caraballo R, Thorsell A-G, Karlberg T, Spjut S, Linusson A, Schüler H, Elofsson M (2015) Towards small molecule inhibitors of mono-ADP-ribosyltransferases. European Journal of Medicinal Chemistry, 95, 546–551. 10.1016/j.ejmech.2015.03.067.

Eustermann S, Wu W-F, Langelier M-F, Yang J-C, Easton LE, Riccio AA, Pascal JM, Neuhaus D (2015): Structural Basis of Detection and Signaling of DNA Single-Strand Breaks by Human PARP-1. Molecular Cell, 60, 742–754. 10.1016/j.molcel.2015.10.032.

Feijs KL, Kleine H, Braczynski A, Forst AH, Herzog N, Verheugd P, Linzen U, Kremmer E, Lüscher B (2013) ARTD10 substrate identification on protein microarrays: regulation of GSK3β by mono-ADP-ribosylation. Cell Communication and Signaling : CCS, 11, 5. 10.1186/1478-811X-11-5.

Flohr C, Bürkle A, Radicella JP, Epe B (2003) Poly(ADP-ribosyl)ation accelerates DNA repair in a pathway dependent on Cockayne syndrome B protein. Nucleic Acids Research, 31, 5332–5337. 10.1093/nar/gkg715

Fujita K, Kubota Y, Ishida H, Sasaki Y (2015) Irinotecan, a key chemotherapeutic drug for metastatic colorectal cancer. World Journal of Gastroenterology, 21, 12234–12248. 10.3748/wjg.v21.i43.12234.

Gagné J-P, Ethier C, Defoy D, Bourassa S, Langelier M-F, Riccio AA, Pascal JM, Moon K-M, Foster LJ, Ning Z, Figeys D, Droit A, Poirier GG (2015): Quantitative site-specific ADP-ribosylation profiling of DNA-dependent PARPs. DNA Repair, 30, 68–79. 10.1016/j.dnarep.2015.02.004.

Gavande NS, VanderVere-Carozza PS, Hinshaw HD, Jalal SI, Sears CR, Pawelczak KS, Turchi JJ (2016) DNA repair targeted therapy: The past or future of cancer treatment? Pharmacology & Therapeutics, 160, 65–83. 10.1016/j.pharmthera.2016.02.003.

Gibbs-Seymour I, Fontana P, Rack JGM, Ahel I (2016): HPF1/C4orf27 Is a PARP-1-Interacting Protein that Regulates PARP-1 ADP-Ribosylation Activity. Molecular Cell, 62. 432–442. 10.1016/j.molcel.2016.03.008.

Gomaa I, Abdel Gaber S, Bhatt S, Liehr T, Glei M, El-Tayeb T, Abdel kader M (2015) In vitro cytotoxicity and genotoxicity studies of gold nanoparticles-mediated photo-thermal therapy versus 5-fluorouracil. Journal of Nanoparticle Research, 17, 102. 10.1007/s11051-015-2912-x.

Han MK, Lee JY, Cho YS, Song YM, An NH, Kim HR, Kim UH (1996) Regulation of NAD+ glycohydrolase activity by NAD(+)-dependent auto-ADP-ribosylation. The Biochemical Journal, 318 (Pt 3), 903–908. 10.1042/bj3180903

Herceg Z, Murr R (2011) Chapter 3 - Mechanisms of Histone Modifications In: Tollefsbol, T (ed): Handbook of Epigenetics. Academic Press, San Diego, pp. 25–45.

Herzog N, Hartkamp JDH, Verheugd P, Treude F, Forst AH, Feijs KLH, Lippok BE, Kremmer E, Kleine H, Lüscher B (2013) Caspase-dependent cleavage of the mono-ADP-ribosyltransferase ARTD10 interferes with its pro-apoptotic function. FEBS Journal, 280. 1330–1343. 10.1111/febs.12124.

Holechek J, Lease R, Thorsell A-G, Karlberg T, McCadden C, Grant R, Keen A, Callahan E, Schüler H, Ferraris D (2018): Design, synthesis and evaluation of potent and selective inhibitors of mono-(ADP-ribosyl)transferases PARP10 and PARP14. Bioorganic & Medicinal Chemistry Letters, 28, 2050–2054. 10.1016/j.bmcl.2018.04.056.

Hu Q, Sun W, Wang C, Gu Z (2016) Recent advances of cocktail chemotherapy by combination drug delivery systems. Advanced Drug Delivery Reviews, 98, 19–34. 10.1016/j.addr.2015.10.022.

Jandu H, Aluzaite K, Fogh L, Thrane SW, Noer JB, Proszek J, Do KN, Hansen SN, Damsgaard B, Nielsen SL, Stougaard M, Knudsen BR, Moreira J, Hamerlik P, Gajjar M, Smid M, Martens J, Foekens J, Pommier Y, Brünner N, Schrohl A-S, Stenvang J (2016) Molecular characterization of irinotecan (SN-38) resistant human breast cancer cell lines. BMC Cancer, 16. 10.1186/s12885-016-2071-1.

Kleine H, Herrmann A, Lamark T, Forst AH, Verheugd P, Lüscher-Firzlaff J, Lippok B, Feijs KL, Herzog N, Kremmer E, Johansen T, Müller-Newen G, Lüscher B (2012) Dynamic subcellular localization of the mono-ADP-ribosyltransferase ARTD10 and interaction with the ubiquitin receptor p62. Cell Communication and Signaling : CCS, 10, 28. 10.1186/1478-811X-10-28.

Kleine H, Poreba E, Lesniewicz K, Hassa PO, Hottiger MO, Litchfield DW, Shilton BH, Lüscher B (2008) Substrate-assisted catalysis by PARP10 limits its activity to mono-ADP-ribosylation. Molecular Cell, 32, 57–69. 10.1016/j.molcel.2008.08.009.

Kumar GK, Prabhakar NR (2008) Post-translational modification of proteins during intermittent hypoxia. Respiratory physiology & neurobiology, 164, 272–276. 10.1016/j.resp.2008.05.017.

Langelier M-F, Planck JL, Roy S, Pascal JM (2012): Structural basis for DNA-dependent poly(ADP-ribosyl)ation by human PARP-1. Science (New York, NY), 336, 728–732. 10.1126/science.1216338.

Leidecker O, Bonfiglio JJ, Colby T, Zhang Q, Atanassov I, Zaja R, Palazzo L, Stockum A, Ahel I, Matic I (2016) Serine is a new target residue for endogenous ADP-ribosylation on histones. Nature Chemical Biology, 12, 998–1000. 10.1038/nchembio.2180.

Li L, Fridley B, Kalari K, Jenkins G, Batzler A, Safgren S, Hildebrandt M, Ames M, Schaid D, Wang L (2008) Gemcitabine and cytosine arabinoside cytotoxicity: association with lymphoblastoid cell expression. Cancer research, 68, 7050–7058. 10.1158/0008-5472.CAN-08-0405.

Li X, Kong X, Kong X, Wang Y, Yan S, Yang Q (2013) 53BP1 Sensitizes Breast Cancer Cells to 5-Fluorouracil. PLoS ONE, 8. 10.1371/journal.pone.0074928.

Liu C, Yu X (2015) ADP-Ribosyltransferases and Poly ADP-Ribosylation. Current protein & peptide science, 16, 491–501. 10.2174/1389203716666150504122435

Liu L, Kong M, Gassman NR, Freudenthal BD, Prasad R, Zhen S, Watkins SC, Wilson SH, Van Houten B (2017): PARP1 changes from three-dimensional DNA damage searching to one-dimensional diffusion after auto-PARylation or in the presence of APE1. Nucleic Acids Research, 45, 12834–12847. 10.1093/nar/gkx1047.

Makogon N, Voznesenskaya T, Bryzgina T, Sukhina V, Grushka N, Alexeyeva I (2010) Poly(ADP–ribose) polymerase inhibitor, 3–aminobenzamide, protects against experimental immune ovarian failure in mice. Reproductive Biology, 10, 215–226. 10.1016/S1642-431X(12)60041-2.

Momparler RL (2013) Optimization of cytarabine (ARA-C) therapy for acute myeloid leukemia. Experimental Hematology & Oncology, 2, 20. 10.1186/2162-3619-2-20.

Montano R, Chung I, Garner KM, Parry D, Eastman A (2012) Preclinical Development of the Novel Chk1 Inhibitor SCH900776 in Combination with DNA Damaging Agents and Antimetabolites. Molecular Cancer Therapeutics, 11, 427–438. 10.1158/1535-7163.MCT-11-0406.

Morgan RK, Carter-O'Connell I, Cohen MS (2015) Selective inhibition of PARP10 using a chemical genetics strategy. Bioorganic & Medicinal Chemistry Letters, 25, 4770–4773. 10.1016/j.bmcl.2015.07.033.

Mouw KW, Goldberg MS, Konstantinopoulos PA, D'Andrea AD (2017) DNA Damage and Repair Biomarkers of Immunotherapy Response. Cancer Discovery, 7, 675–693. 10.1158/2159-8290.CD-17-0226.

Morgan RK, Kirby IT, Vermehren-Schmaedick A, Rodriguez K, Cohen MS (2019): Rational Design of Cell-Active Inhibitors of PARP10. ACS Medicinal Chemistry Letters, 10, 74–79. 10.1021/acsmedchemlett.8b00429.

Munnur D, Ahel I (2017) Reversible mono-ADP-ribosylation of DNA breaks. The FEBS journal, 284, 4002–4016. 10.1111/febs.14297.

Nicolae CM, Aho ER, Vlahos AHS, Choe KN, De S, Karras GI, Moldovan G-L (2014) The ADP-ribosyltransferase PARP10/ARTD10 interacts with proliferating cell nuclear antigen (PCNA) and is required for DNA damage tolerance. The Journal of Biological Chemistry, 289, 13627–13637. 10.1074/jbc.M114.556340.

Peterson LE, Kovyrshina T (2019) DNA Repair Gene Expression Adjusted by the PCNA Metagene Predicts Survival in Multiple Cancers. Cancers. 11, 501. 10.3390/cancers11040501.

Prasad CB, Prasad SB, Yadav SS, Pandey LK, Singh S, Pradhan S, Narayan G (2017) Olaparib modulates DNA repair efficiency, sensitizes cervical cancer cells to cisplatin and exhibits anti-metastatic property. Scientific Reports, 7. 10.1038/s41598-017-13232-3.

Putt KS, Hergenrother PJ (2004) An enzymatic assay for poly(ADP-ribose) polymerase-1 (PARP-1) via the chemical quantitation of NAD+: application to the high-throughput screening of small molecules as potential inhibitors. Analytical Biochemistry, 326, 78–86. 10.1016/j.ab.2003.11.015.

Rakhimova A, Ura S, Hsu D-W, Wang H-Y, Pears CJ, Lakin ND (2017) Site-specific ADP-ribosylation of histone H2B in response to DNA double strand breaks. Scientific Reports, 7. 43750. 10.1038/srep43750.

Rasheed ZA, Rubin EH (2003) Mechanisms of resistance to topoisomerase I-targeting drugs. Oncogene, 22, 7296–7304. 10.1038/sj.onc.1206935.

Sánchez-Alcázar J, Khodjakov A, Schneider E (2001) Anticancer drugs induce increased mitochondrial cytochrome c expression that precedes cell death. Cancer research, 61. 1038–1044.

Schleicher EM, Galvan AM, Imamura-Kawasawa Y, Moldovan G-L, Nicolae CM (2018a) PARP10 promotes cellular proliferation and tumorigenesis by alleviating replication stress. Nucleic Acids Research, 46, 8908–8916. 10.1093/nar/gky658.

Schuller M, Riedel K, Gibbs-Seymour I, Uth K, Sieg C, Gehring AP, Ahel I, Bracher F, Kessler BM, Elkins JM, Knapp S (2017): Discovery of a selective allosteric inhibitor targeting macrodomain 2 of poly-adenosine-diphosphate-ribose polymerase 14. ACS chemical biology, 12, 2866–2874. 10.1021/acschembio.7b00445.

Shahabi J, Shahmabadi E, Alavi SE, Movahedi F, Koohi M, Zadeh Mehrizi T, Akbarzadeh A (2014) Effect of Gold Nanoparticles on Properties of Nanoliposomal Hydroxyurea: An In Vitro Study. Indian Journal of Clinical Biochemistry, 29, 315–320. 10.1007/s12291-013-0355-7.

Shahrour MA, Nicolae CM, Edvardson S, Ashhab M, Galvan AM, Constantin D, Abu-Libdeh B, Moldovan G-L, Elpeleg O (2016) PARP10 deficiency manifests by infantile neurodegeneration and DNA repair defect. Neurogenetics, 17, 227–232. 10.1007/s10048-016-0493-1.

Siegel C, McCullough LD (2011) NAD+ Depletion or PAR Polymer Formation: Which Plays the Role of Executioner in Ischemic Cell Death? Acta physiologica (Oxford, England), 203, 225–234. 10.1111/j.1748-1716.2010.02229.x.

Strasser S, Maier S, Leisser C, Saiko P, Madlener S, Bader Y, Bernhaus A, Gueorguieva M, Richter S, Mader RM, Wesierska-Gadek J, Schott H, Szekeres T, Fritzer-Szekeres M, Krupitza G (2006) 5-FdUrd–araC heterodinucleoside re-establishes sensitivity in 5-FdUrd- and AraC-resistant MCF-7 breast cancer cells overexpressing ErbB2. Differentiation, 74, 488–498. 10.1111/j.1432-0436.2006.00082.x.

Sukhanova MV, Khodyreva SN, Lebedeva NA, Prasad R, Wilson SH, Lavrik OI (2005): Human base excision repair enzymes apurinic/apyrimidinic endonuclease1 (APE1), DNA polymerase β and poly(ADP-ribose) polymerase 1: interplay between strand-displacement DNA synthesis and proofreading exonuclease activity. Nucleic Acids Research, 33, 1222–1229. 10.1093/nar/gki266.

Thorsell A-G, Ekblad T, Karlberg T, Löw M, Pinto AF, Trésaugues L, Moche M, Cohen MS, Schüler H (2017) Structural Basis for Potency and Promiscuity in Poly(ADP-ribose) Polymerase (PARP) and Tankyrase Inhibitors. Journal of medicinal chemistry, 60, 1262–1271. 10.1021/acs.jmedchem.6b00990.

Trucco C, Oliver FJ, de Murcia G, Ménissier-de Murcia J (1998): DNA repair defect in poly(ADP-ribose) polymerase-deficient cell lines. Nucleic Acids Research, 26, 2644–2649. 10.1093/nar/26.11.2644

Tutt A, Robson M, Garber JE, Domchek SM, Audeh MW, Weitzel JN, Friedlander M, Arun B, Loman N, Schmutzler RK, Wardley A, Mitchell G, Earl H, Wickens M, Carmichael J (2010) Oral poly(ADP-ribose) polymerase inhibitor olaparib in patients with BRCA1 or BRCA2 mutations and advanced breast cancer: a proof-of-concept trial. The Lancet, 376, 235–244. 10.1016/S0140-6736(10)60892-6.

Venkannagari H, Fallarero A, Feijs KLH, Lüscher B, Lehtiö L (2013) Activity-based assay for human mono-ADP-ribosyltransferases ARTD7/PARP15 and ARTD10/PARP10 aimed at screening and profiling inhibitors. European Journal of Pharmaceutical Sciences: Official Journal of the European Federation for Pharmaceutical Sciences, 49, 148–156. 10.1016/j.ejps.2013.02.012.

Venkannagari H, Verheugd P, Koivunen J, Haikarainen T, Obaji E, Ashok Y, Narwal M, Pihlajaniemi T, Lüscher B, Lehtiö L (2016) Small-Molecule Chemical Probe Rescues Cells from Mono-ADP-Ribosyltransferase ARTD10/PARP10-Induced Apoptosis and Sensitizes Cancer Cells to DNA Damage. Cell Chemical Biology, 23, 1251–1260. 10.1016/j.chembiol.2016.08.012.

Verdone L, La Fortezza M, Ciccarone F, Caiafa P, Zampieri M, Caserta M (2015) Poly(ADP-Ribosyl)ation Affects Histone Acetylation and Transcription. PloS One, 10, e0144287. 10.1371/journal.pone.0144287.

Verheijen M, Lienhard M, Schrooders Y, Clayton O, Nudischer R, Boerno S, Timmermann B, Selevsek N, Schlapbach R, Gmuender H, Gotta S, Geraedts J, Herwig R, Kleinjans J, Caiment F (2019) DMSO induces drastic changes in human cellular processes and epigenetic landscape in vitro. Scientific Reports, 9, 4641. 10.1038/s41598-019-40660-0.

Verheugd P, Forst AH, Milke L, Herzog N, Feijs KLH, Kremmer E, Kleine H, Lüscher B (2013) Regulation of NF-κB signalling by the mono-ADP-ribosyltransferase ARTD10. Nature Communications, 4, 1683. 10.1038/ncomms2672.

Vyas S, Chesarone-Cataldo M, Todorova T, Huang Y-H, Chang P (2013) A systematic analysis of the PARP protein family identifies new functions critical for cell physiology. Nature communications, 4, 2240. 10.1038/ncomms3240.

Vyas S, Matic I, Uchima L, Rood J, Zaja R, Hay RT, Ahel I, Chang P (2014) Family-wide analysis of poly(ADP-ribose) polymerase activity. Nature communications, 5, 4426. 10.1038/ncomms5426.

Yang C-S, Jividen K, Spencer A, Dworak N, Ni L, Oostdyk LT, Chatterjee M, Kusmider B, Reon B, Parlak M, Gorbunova V, Abbas T, Jeffery E, Sherman NE, Paschal BM (2017) Ubiquitin Modification by the E3 Ligase/ADP-ribosyltransferase Dtx3L/Parp9. Molecular cell, 66, 503-516.e5. 10.1016/j.molcel.2017.04.028.

Yoneda KY, Cross CE (2010) 8.24 - The Pulmonary Toxicity of Anticancer Agents In: McQueen, CA (ed): Comprehensive Toxicology (Second Edition). Elsevier, Oxford, pp. 477–510.

Yu M, Schreek S, Cerni C, Schamberger C, Lesniewicz K, Poreba E, Vervoorts J, Walsemann G, Grötzinger J, Kremmer E, Mehraein Y, Mertsching J, Kraft R, Austen M, Lüscher-Firzlaff J, Lüscher B (2005) PARP-10, a novel Myc-interacting protein with poly(ADP-ribose) polymerase activity, inhibits transformation. Oncogene, 24, 1982–1993. 10.1038/sj.onc.1208410.

Yu M, Zhang C, Yang Y, Yang Z, Zhao L, Xu L, Wang R, Zhou X, Huang P (2011) The interaction between the PARP10 protein and the NS1 protein of H5N1 AIV and its effect on virus replication. Virology Journal, 8, 546. 10.1186/1743-422X-8-546.

Electronic sources

Cell atlas - PARP10 - The Human Protein Atlas.
URI: https://www.proteinatlas.org/ENSG00000178685-PARP10/cell. Cited 2019/4/24.

Expression Atlas, search results.
URI:
https://www.ebi.ac.uk/gxa/search?geneQuery=%5B%7B%22value%22%3A%22PARP10%22%7D%5D&species=homo%20sapiens&conditionQuery=%5B%7B%22value%22%3A%22HeLa%22%7D%2C%7B%22value%22%3A%22MDA-MB-231%22%7D%2C%7B%22value%22%3A%22MCF7%22%7D%5D&bs=%7B%22homo%20sapiens%22%3A%5B%22CELL_LINE%22%5D%7D&ds=%7B%22kingdom%22%3A%5B%22animals%22%5D%7D#baseline. Cited 2019/5/9.

PubChem. 4-(4-Carbamoylphenoxy)benzamide.
URI: https://pubchem.ncbi.nlm.nih.gov/compound/236501. Cited 2019/4/24.

Sigma-Aldrich. 5-Fluorouracil F6627.
URI: https://www.sigmaaldrich.com/catalog/product/sigma/f6627. Cited 2019/4/24.
Sigma-Aldrich. Cytosine β-<SC>D</SC>-arabinofuranoside C1768.
URI: https://www.sigmaaldrich.com/catalog/product/sigma/c1768. Cited 2019/4/24.

Sigma-Aldrich. Dimethyl sulfoxide.
URI:
https://www.sigmaaldrich.com/catalog/substance/dimethylsulfoxide78136768511?lang=fi&region=FI&attrlist=Brand. Cited 2019/4/24.
Sigma-Aldrich. Hydroxyurea H8627.
URI: https://www.sigmaaldrich.com/catalog/product/sigma/h8627. Cited 2019/4/24.
Sigma-Aldrich. Irinotecan hydrochloride I1406.
URI: https://www.sigmaaldrich.com/catalog/product/sigma/i1406. Cited 2019/4/24.

Sigma-Aldrich. Teniposide SML0609.
URI: https://www.sigmaaldrich.com/catalog/product/sigma/sml0609. Cited 2019/4/24.

Appendix

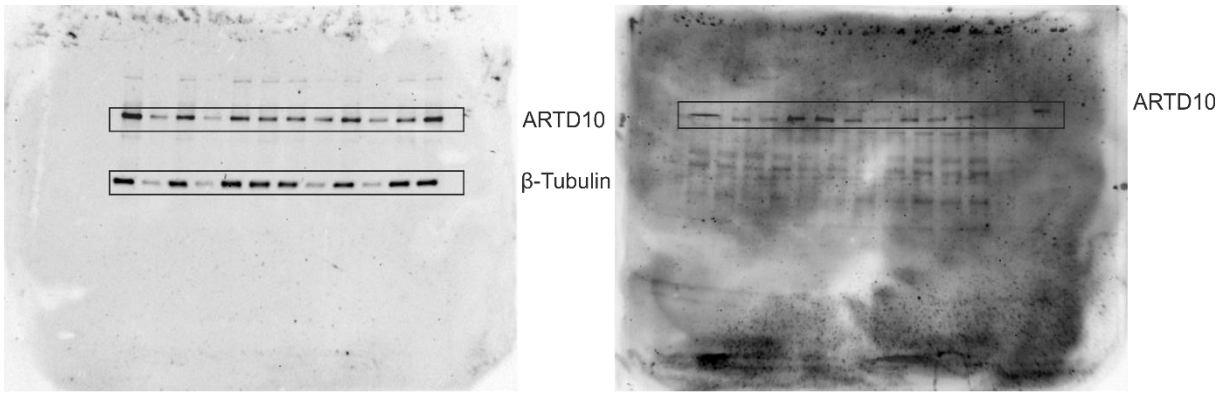

Examples of western blot membranes (MDA-MB-231 cells). A represents the western blot membrane with ARTD10 from cytoplasmic fraction merged with loading control image. For this image, 180.0 second exposure time was used in case of ARTD10 bands, and in case of β-tubulin bands, 2.5 seconds. B represents a western blot membrane containing nuclear fractions merged with loading control image. On this image, 600.0 second exposure was used both in case of ARTD10 and non-detectable H3 bands. All fractions of this image are obtained after 24h of compound administrations. The bands of interest are marked with rectangle, and the names of proteins are displayed next to the membrane images.